Optimized Spatial Configuration of Heterogeneous Biocatalysts Maximizes Cell-Free Biosynthesis of ω-Hydroxy and ω-Amino Acids

Javier Santiago-Arcos[a], *Susana Velasco-Lozano*[a,b,e]*, *Eleftheria Diamanti*[a], *Ana I. Benítez-Mateos*[c,d], *Daniel Grajales-Hernández*[a], *Francesca Paradisi*[c], *and Fernando López-Gallego*[a,f]*

[a] Heterogeneous Biocatalysis group, CIC biomaGUNE, Edificio Empresarial "C", Paseo de Miramón 182, 20009, Donostia, Spain.

[b] Instituto de Síntesis Química y Catálisis Homogénea (ISQCH), CSIC-Universidad de Zaragoza, C/ Pedro Cerbuna, 12, 50009, Zaragoza, Spain.

[c] Department of Chemistry, Biochemistry and Pharmaceutical Sciences, University of Bern, Freiestrasse 3, 3012, Bern, Switzerland.

[d] Current address: Department of Chemistry and Applied Sciences, ETH Zürich, Vladimir-Prelog-Weg 1, 8093, Zürich, Switzerland.

[e] Aragonese Foundation for Research and Development (ARAID), Zaragoza (Spain).

[f] IKERBASQUE, Basque Foundation for Science, Bilbao (Spain).

*Corresponding authors. (F. López-Gallego) and (S. Velasco-Lozano)

Phone: +34 943003500 Ext 309

E-mail addresses: flopez@cicbiomagune.es and svelasco@unizar.es

Keywords: Enzyme immobilization, flow biocatalysis, alcohol dehydrogenases, multi-enzyme cascades, cofactor recycling, hydrogen peroxide

ABSTRACT

Cell-free biocatalysis is gaining momentum in producing value-added chemicals, particularly in stepwise reaction cascades. However, the stability of enzyme cascades in industrial settings is often compromised when using free enzymes. In this study, we have developed a stable multifunctional heterogeneous biocatalyst co-immobilizing five enzymes on microparticles to transform 1,ω-diols into 1,ω-hydroxy acids. We improved the operational efficiency and stability of the heterogeneous biocatalyst by fine-tuning enzyme loading and spatial organization. Stability issues are overcome through post-immobilization polymer coating. The general applicability of this heterogeneous biocatalyst is demonstrated by its scale-up in both batch and packed bed reactors, allowing a product yield of > 80%. The continuous process is fed with H_2O_2 as the oxygen source, reaching a Space-Time Yield (STY) of 0.76 $g \cdot L^{-1} \cdot h^{-1}$, maintained for the first 12 hours. Finally, this flow system is telescoped with a second plug-flow reactor packed with a different heterogeneous biocatalyst. As a result, this 6-enzyme 2-reactor system sequentially transforms 1,ω-diols into 1,ω-aminoacids while *in-situ* recycling NAD^+, depleting H_2O_2 and generating O_2.

INTRODUCTION

Cell-free biocatalysis is gaining momentum in manufacturing value-added chemicals, especially when dealing with multi-step reaction cascades.[1-3] As enzymes often exhibit exquisite selectivity under mild reaction conditions, they are very promising catalysts to be incorporated into synthetic routes for more efficient and sustainable chemical manufacturing.[4] Multi-enzyme cascades allow us to carry out multi-step chemical reactions (simultaneously or sequentially) in one pot, avoiding isolation and purification during the process.[4] Furthermore, the control of activity ratio in enzyme cascades minimizes intermediate inhibitory effects and side-product accumulation that may jeopardize the overall throughput of the cascade.[5] However, the stability of enzyme cascades under industrial operational conditions is normally compromised when using free enzymes. To overcome this issue, enzyme immobilization emerges as a great solution to enhance enzyme stability and allows enzyme recycling once the reaction is completed.[6, 7] Moreover, immobilized enzymes present a greater versatility to be implemented in different types of reactors. Not surprisingly, enzyme immobilization is the key enabling technology revolutionizing flow-biocatalysis.[8-13]

Besides stabilization, enzyme immobilization can also tune the spatial organization of enzymes across the 3D structure of the immobilization supports. Achieving precise spatial rearrangement of enzymes within solid supports is critical for optimizing the performance of any immobilized multi-enzyme system. The strategic colocalization of enzymes may maximize the efficient mass transfer of intermediates and cofactors between various active sites. For example, NADH oxidases immobilized on the outer surface of porous supports present higher activity than those immobilized on the inside due to lower mass transport restrictions to molecular oxygen.[14] Furthermore, another successful example is the co-immobilization of multi-enzyme systems that demand the recycling of cofactors *in*

situ and/or the removal of by-products.[15] However, spatial organization and colocalization of several enzymes imply their co-immobilization on the same support, which is not trivial as enzymes with different physicochemical properties may need different immobilization chemistries. In this context, supports activated with different reactive groups, also named heterofunctional supports, have been successfully applied for the co-immobilization of multi-enzyme systems.[15, 16] The vast majority of heterofunctional supports offer the combination of only two reactive groups; one (i.e., ionic, hydrophobic, metal chelate groups) to drive the enzyme adsorption, and the other (i.e., epoxy, aldehyde, glyoxyl, and vinyl groups) to react with the exposed nucleophilic residues on the enzyme surface to form covalent and irreversible bonds. [17-20] The combination of these two groups allows a two-step enzyme immobilization, in which the enzyme is first absorbed very rapidly (close contact), and then irreversibly attached to the support. As most multi-enzyme systems are composed of multimeric enzymes, the co-immobilization of enzymes on pre-existing heterofunctional supports is unable to fully stabilize their quaternary structure. To that aim, post-immobilization techniques based on enzyme polymer coating are a recurrent strategy to avoid subunit lixiviation of the immobilized enzymes during the operation. The gain in stability when an immobilized enzyme is coated with a polymer brush is widely reported in the literature not only for single enzymes[21] but also for multi-enzyme systems.[15, 16]

The recently developed cell-free biosynthetic cascade that transforms 1,ω-diols into ω-hydroxy acids (ω-HA) is an excellent candidate to benefit from the co-immobilization of the multi-enzyme system through tuning its intraparticle spatial organization.[22] In this 5-enzyme cascade two NAD^+-dependent dehydrogenases (ADHs) synergistically catalyze the double oxidation of 1,ω-diols to their corresponding lactones that are subsequently hydrolyzed by a lactonase (LAC) to yield the target ω-hydroxy acids. The efficiency of

the process relies on the *in-situ* recycling of NAD^+ driven by an NADH oxidase (NOX) that concomitantly produces hydrogen peroxide; a harmful oxidant that is removed by catalase (CAT) to avoid enzyme inactivation. A previous work proposes a similar biosynthetic pathway towards the synthesis of ω-HA from cyclopentane but using resting cells as enzyme chassis. In the whole-cell biotransformation, the maximum product titer is 5 mM concentration of ω-HA **(Scheme 1a)**.[23] In contrast, our cell-free system can increase the product titer 20 times with superior green and sustainable metrics **(Scheme 1b)**.[22] Nevertheless, the incompatibility between the immobilization chemistries needed for each enzyme forced us to heterogenize the system using two different supports where the biosynthetic cascade was physically segregated, having one of the dehydrogenases far away from the NAD^+ recycling system. This segregation yielded lower product titer than the system in solution and presented limited reusability as product yield dramatically decreased after the first operational cycle.[22] Other cell-free systems have accomplished the transformation of cyclic alkyl amines into ω-amino acids through a sequential process coupling transaminases and oxidoreductases (**Scheme 1c**).[24]

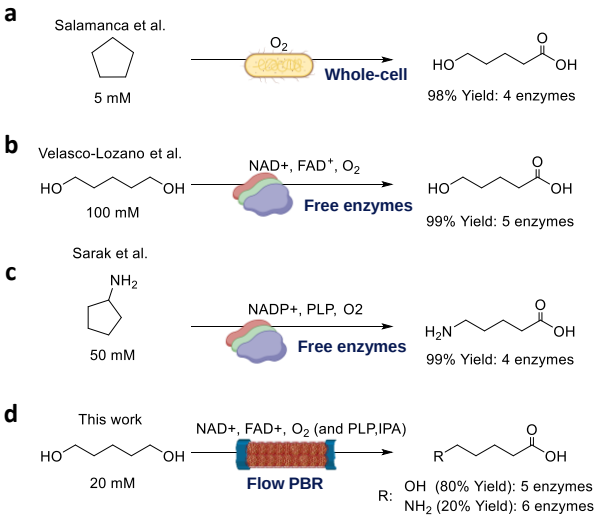

Scheme 1. Different catalytic approaches for the synthesis of 5-Hydroxy or 5-Aminopentanoic acid, **a**; using resting cells in batch. **b** and **c;** using free enzymes in batch. **d**; using immobilized multi-enzyme systems operated in flow.

In this work, we have heterogenized the 5-enzyme system described in **scheme b** using a tri-functional support (AG-Co^{2+}/A/G) developed by our group.[25] This support has proven successful in individually immobilizing the 5 enzymes involved in the biocascade, achieving active and stable heterogeneous biocatalysts for most of them. Enzymes can be immobilized through His-tag coordination, ionic adsorption, and covalent bonds as this support displays cobalt-chelates, positively charged secondary amines, and aldehyde (from glutaraldehyde) groups, respectively. Upon kinetic characterization, the co-immobilized multi-enzyme system was optimized by tuning the intraparticle enzyme spatial distribution, finding the key role of the NOX localization for the overall productivity and stability of the cascade. Finally, the multi-functional heterogeneous biocatalyst was further stabilized by post-immobilization polymeric coating and increasing the NOX/CAT loads. The optimal solid biocatalyst was submitted to a one-pot transformation of 1,5-pentanediol (1,5-PD) as model diol to yield 5-Hydroxypentanoic (5-HP) acid in consecutive batch cycles, demonstrating excellent operational stability and scalability. Finally, we packed this heterogeneous multi-enzyme system in a plug-flow column to set a packed bed reactor for which we optimized the oxygen to maximize both product titer and space-time yield (**Scheme 1d**).

RESULTS AND DISCUSSION

Optimization of the spatial organization in multi-functional heterogeneous biocatalysts

The enzyme cascade is composed of two NAD^+-dependent alcohol dehydrogenases from *Bacillus stearothermophilus* (ADH1)[26] and horse liver (ADH2)[27] to synergistically oxidize 1,5-PD to δ-valerolactone (lactone) via its corresponding lactol intermediate (tetrahydro-2H-pyran-2-ol). As mentioned above, the pool of NAD^+ is replenished by an oxygen-dependent NADH oxidase from *Thermus thermophilus HB27* (NOX)[28] coupled

to a catalase from bovine liver (CAT) that depletes the hydrogen peroxide generated as a by-product of NOX. Finally, a lactonase from *Sulfolobus islandicus* (LAC)[29] hydrolyzes δ-valerolactone (Tetrahydro-2H-pyran-2-one) to 5-HP **(Figure 1a)**. In a previous work, this multi-enzyme system showed very promising conversion yields by optimizing the enzyme ratio to overcome the bottleneck of the reaction (the oxidation of the lactol into the lactone).[22] However, we encountered issues when trying to scale up the reaction (from 2 mL to 10 and 25 mL) due to enzyme instability. To overcome these issues, we (co)-immobilized the 5 free enzymes involved in the cascade on the tri-functional support described above (AG-Co^{2+}/A/G) following different spatial configurations **(Table 1)**. While ADH1 and LAC are immobilized through their His-tags reacting with the cobalt-chelates, CAT, and ADH2 establish electrostatic interactions with the positively charged secondary amines of the carrier, and NOX forms covalent bonds between its surface lysines and the aldehyde groups displayed at the carrier surface. First, we individually immobilized all enzymes on the same support resulting in five monofunctional heterogeneous biocatalysts (HB1 to HB5). In this configuration each enzyme is immobilized on a bead different from the others, naming this spatial distribution as D1 **(Entry 1, Table 1)**. Secondly, ADH1 and ADH2 were immobilized separately on AG-Co^{2+}/A/G but co-immobilized with NOX and CAT resulting in biocatalysts HB6 and HB7, respectively, and finally mixed with LAC immobilized on AG-Co^{2+}/A/G by its own (HB5) to assemble the configuration D2 (**Entry 2, Table 1**). Thirdly, NOX and CAT were co-immobilized with both ADHs (ADH1 and ADH2) on AG-Co^{2+}/A/G yielding the heterogeneous biocatalyst HB8 that was mixed with HB5 containing only LAC to assemble configuration 3, D3 (**Entry 3, Table 1**). Finally, the five enzymes were sequentially co-immobilized on AG-Co^{2+}/A/G to prepare biocatalyst HB9 with a configuration 4, D4 (**Entry 4, Table 1**). All HBs were incubated with 1 M glycine upon

Table 1. Immobilization parameters of enzymes bound to AG-Co^{2+}/A/G with different spatial distribution, enzyme loads, and polymer coatings

Entry	Distribution	Heterogeneous biocatalyst	Enzyme	Enzyme load ($mg \cdot g^{-1}$)	Ψ [a] (%)	Recovered activity [b] ($U \cdot g^{-1}$) /(%)
1	D1	HB1	ADH2	15[c]	100	0.42 (23)
		HB2	NOX	0.41	81	0.67 (5)
		HB3	CAT	0.010[c]	40	107 (25)
		HB4	ADH1	5	100	1.52 (11)
		HB5	LAC	1.49	98	0.35 (21)
2	D2	HB6	ADH2	7.4 [c]	99	0.5 (26)
			NOX	0.21	33	0.21 (15)
			CAT	0.004	56	109.7 (26)
		HB7	ADH1	2.45	98	1.19 (28)
			NOX	0.12	94	0.67 (5)
			CAT	0.004	65	127.3 (30)
		HB5	LAC	1.49	98	0.35 (21)
3	D3	HB8	ADH2	4.20[c]	99	na (na)
			NOX	0.13	57	0.40 (20)
			CAT	0.004	38	237 (61)
			ADH1	1.26	100	0.66 (23)
		HB5	LAC	1.49	98	0.35 (21)
4	D4	HB9	ADH2	3.0[c]	100	na (na)
			NOX	0.12	65	0.53 (30)
			CAT	0.0023	19	343 (36)
			ADH1	1.0	100	0.9 (50)
			LAC	0.30	85	0.33 (46)
5	[d]D5	HB10	ADH2	3.0[c]	100	na (na)
			NOX	0.14	79	0.50 (26)
			CAT	0.12[c]	99	104 (8)
			ADH1	0.99	99	1.08 (50)
			LAC	0.32	100	0.18 (23)
6	[d]D5	HB11	ADH2	3.0[c]	100	na (na)
			NOX	0.15	82	0.51 (26)
			CAT	0.12[c]	99	120 (9)
			ADH1	1.0	100	1.04 (47)
			LAC	0.32	100	0.18 (23)
7	[d]D5	HB12	ADH2	3.0[c]	100	na (na)
			NOX	0.66	74	1.25 (17)
			CAT	0.87[c]	73	770 (35)
			ADH1	1.0	100	1.07 (49)
			LAC	0.32	100	0.20 (25)
8	[d]D5	HB13	ADH2	3.0[c]	100	na (na)
			NOX	0.72	80	1.7 (20)
			CAT	1.14	95	116 (5)

ADH1	1.0	100	1.5 (53)
LAC	0.32	100	0.26 (32)

[a] Immobilization yield, Ψ = (immobilized activity/offered activity) × 100. [b] (%) Recovered activity of the immobilized enzyme is defined as the coefficient between the specific activity of the immobilized enzymes and the specific activity of the soluble ones. [c] Total protein content in a semi-purified enzyme extract. [d]D5 is the distribution where the 5 enzymes are co-immobilized and co-localized at the outer region of the same bead. All data herein presented correspond to the mean value of three independent enzyme activity and protein concentration assays. In all cases, the standard deviation was never higher than 5% of the mean value.

2 h of enzyme immobilization to block the remaining aldehydes which do not intervene in the enzyme attachment.

These four spatial distributions imply that intermediates must follow different interparticle diffusion pathways toward the final product. Accordingly, in D1 all intermediates must travel from one particle to the other to be processed by their corresponding enzyme **(Figure 1b)**. In contrast, as D2 segregates each oxidation step but confines the NAD^+ recycling and H_2O_2 removal, the only intermediates forced to travel between particles are the lactol and the lactone (**Figure S1a**). In the case of D3, only the lactone must diffuse between different particles to be hydrolyzed by LAC (**Figure S1b**). Finally, as D4 confines the five enzymes inside the same particle, interparticle transport of intermediates is not needed to complete the cascade target product (**Figure 1c**). Expectedly, the immobilization parameters for each enzyme varied depending on whether the enzymes were individually immobilized or co-immobilized together (**Table 1**). This phenomenon was already reported for ADH1, whose recovered activity when immobilized alone is different from the activity recovered when co-immobilized with other enzymes.[30]

Once the 9 different HBs (HB1-9) were prepared, they were mixed to assemble the multi-enzyme systems with the corresponding spatial distribution (D1-D4) in reaction, keeping a protein mass ratio of 1:3:0.18:0.012:0.32 for ADH1:ADH2:NOX:CAT:LAC,

respectively. We selected that protein mass ratio because it resulted in the highest yield of ω-HA when the cascade was catalyzed by the same free enzymes.[22] Monitoring the reaction courses, we observed that D1 and D4 converted 75% of 1,5-PD (16.3 mM) yielding up to 60% of 5-HP (11.8 mM) in 24 h (**Figures 1b and 1c**), whereas D2 and D3 only reached a 32% (6.4 mM) and 35% (7.2 mM) 5-HP yield, respectively, after the same time (**Figures S1a and S1b**). Remarkably, **Figure 1d** shows that all enzymes co-immobilized on the same particle (**Entry 4, Table 1**) transform 1,5-PD into 5-HP 1.6 times faster than all enzymes physically segregated into different particles (**Entry 1, Table 1**). Since the oxidation of the lactol intermediate is the rate-limiting step in this cascade due to the high apparent K_M of ADH2 towards it,[31] its greater accumulation using the HB9 with D4 configuration may speed up the lactone production, thus contributing to improving the overall throughput of the cascade when using this spatial configuration. As the D1 and D4 configurations present the most promising results in terms of product yield and productivity, we discarded the D2 and D3 configurations for further studies.

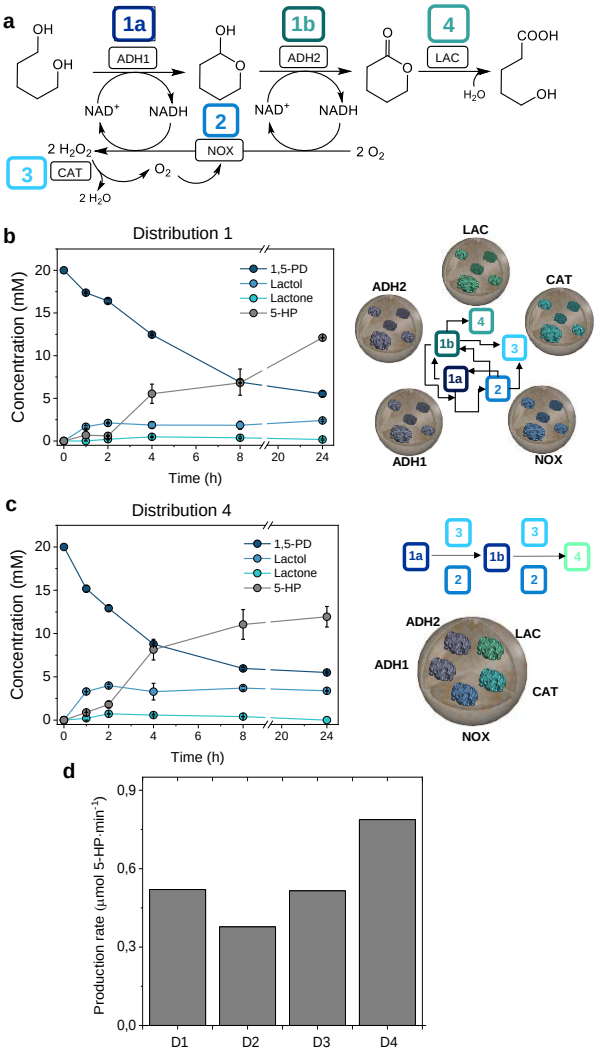

Figure 1. Effect of the spatial organization on the performance of different HBs for the batch biosynthesis of 5-HP. **a,** Reaction scheme. **b,c,** Reaction time courses catalyzed using Distribution 1(**b**), individually immobilized enzymes in different particles, or Distribution 4 (c), co-immobilized multi-enzyme system in the same particle. In the right panels, the interparticle (b) or the intraparticle diffusion of the intermediates between the different enzymes. Data in panels b and c represent the mean value and standard deviation (error bars) of two independent experiments. **d**, Maximum production rate of 5-HP achieved with different multifunctional heterogeneous biocatalysts with different spatial distribution (D1-D4). The maximum production rate was calculated in the first 4 h of the reaction course. In all cases, the reaction mixture consisted of 20 mM 1,5-PD, 1 mM NAD^+, and 0.15 mM FAD^+ dissolved in 100 mM sodium phosphate buffer pH 8. The employed FAD^+ concentration was based on a previously reported optimization where the NOX enzyme displays the highest specific activity.[28]

Operational stability of the heterogeneous multi-functional biocatalyst with different spatial configurations.

Due to the promising performance of HBs under D1 and D4 spatial configurations, we tested their operational stability in consecutive batch reaction cycles by assessing the cascade coupling (**Figure 2**). This latter parameter is defined as the produced mol of 5-HP per consumed mol of 1,5-PD, where the ideal system would reach a coupling efficiency value of 1, indicating a perfect cascade orchestration where the substrate (1,5-PD) and intermediates (lactol and lactone) are quantitatively converted into the final target product (5-HP). Although HB9 with configuration D4 (**Entry 4, Table 1**) outperforms HB1-5 in configuration D1 (**Entry 1, Table 1**) for the first cycle, the cascade coupling efficiency was higher with D1 than with D4 in the second and third consecutive cycles, pointing out that the 5 enzymes co-immobilized together are less stable than those separately immobilized on the same support (**Figure 2a**). To understand the lower operational stability of the co-immobilized system (D4), we investigated the catalytic efficiency of each cascade step using a set of spectrophotometric assays that allowed us to determine the activity of the diol oxidation (**Figure S2a**), the NADH oxidation (**Figure S2b**), the hydrogen peroxide accumulation (**Figure S3**) and the ω-hydroxy acid production (**Figure S4**). **Figure 2b** shows that HB9 in configuration D4 is 3 and 4 times faster for the diol oxidation and NADH recycling, respectively than the configuration D1 using HB1-5. These results match the reaction time courses (**Figure 1**), supporting the higher overall throughput of this cascade when it is catalyzed by the 5-enzymes co-immobilized on the same porous particle of AG-Co^{2+}/A/G. However, the D4 spatial configuration accumulates H_2O_2 5 times faster than the configuration D1, suggesting that CAT in the co-immobilized system cannot match the activity of the NOX. As H_2O_2 is a liaison for enzymes, its accumulation in the reaction catalyzed by HB9 in configuration

D4 explains the system inactivation during the process. Despite the unsatisfactory operational stability, the high efficiency of the co-immobilized biocatalysts encouraged us to enhance its operational stability by optimizing its capacity to remove the H_2O_2 formed *in situ*, without limiting the NADH recycling.

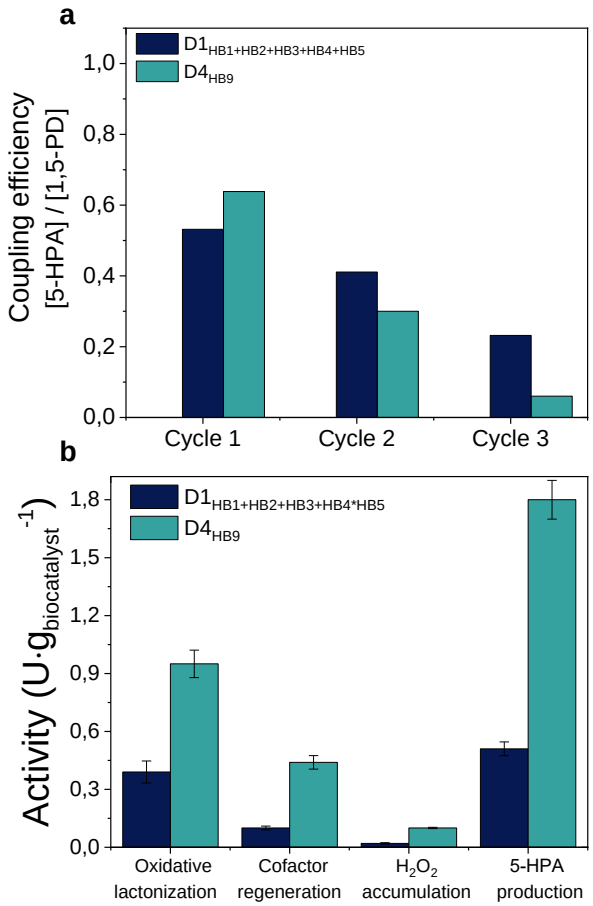

Figure 2. Effect of the enzyme system distribution on the performance of HBs for batch 5-HP biosynthesis. **a**, Coupling efficiency after consecutive batch cycles performed with HBs with distributions D1 and D4. **b**, Individual activities of different reaction steps determined spectrophotometrically for HBs with distribution D1 and D4 (see supplementary information for more details). Data in panel b corresponds to the mean value and standard deviation (error bars) of triplicate activity assays.

Optimization of the intraparticle spatial distribution and loading of 5-enzymes co-immobilized system to maximize its performance.

To investigate why hydrogen peroxide is accumulated when the cascade is catalyzed by HB9 in configuration D4, we studied the intraparticle spatial distribution of a co-immobilized enzyme system by confocal laser scanning microscopy (CLSM) using enzymes labeled with compatible fluorophores for colocalization studies. **Figures 3a** and **S5** show that four of the co-immobilized enzymes are located at the outer surface of the particle, whereas NOX is located at the inner regions of the beads. This spatial distribution agrees with the spatial distribution found for the five enzymes individually immobilized on this support (**Figure S6**), as previously reported.[25] The intra-particle segregation of NOX and CAT may explain their impaired activities. Thus, the hydrogen peroxide can accumulate during biotransformation as it is produced at large distances (inner regions of the particle) from where it can be removed (outer regions of the particle), damaging the co-immobilized enzymes.

To improve the hydrogen peroxide removal, we optimized the spatial distribution of NOX by tuning its immobilization kinetics, colocalizing all 5 enzymes at the outer surface of the beads. As previously demonstrated, high enzyme immobilization rates yield immobilized enzymes located at the outer parts of microbeads,[32] while slowly immobilized enzymes are uniformly distributed across the beads. The immobilization rate can be easily controlled by either adding immobilization competitors or modifying the immobilization buffer and/or conditions. To favor a more rapid NOX immobilization rate and enable its localization at the outer surface of the beads, we performed its immobilization on AG-Co^{2+}/A/G in the presence of a gradient of NaCl concentration (0, 0.1, 0.5, and 1 M).

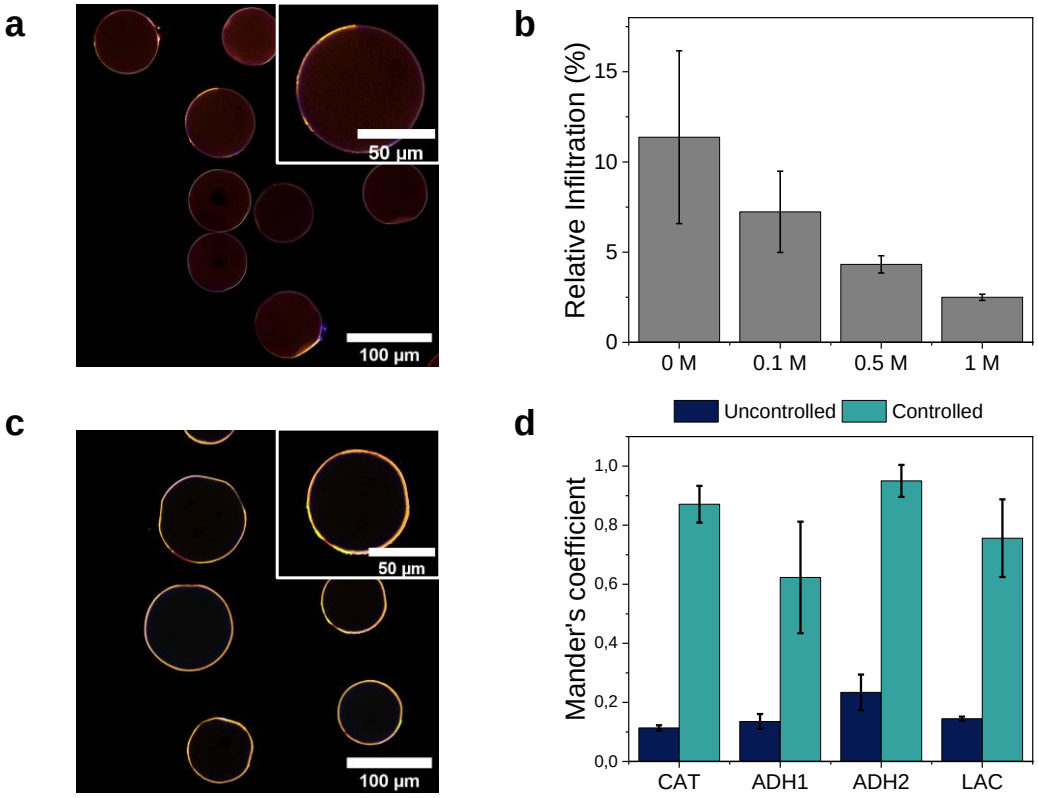

Figure 3. Intraparticle spatial organization of enzymes. **a**, Merged CLSM images of a 5-enzyme system co-immobilized in the absence of NaCl (HB9). **b**, Relative infiltration of NOX through the radius of AG-Co^{2+}/A/G beads when immobilized at different NaCl concentrations (HB10). **c**, Merged CLSM images of a 5-enzyme system co-immobilized in the presence of 1 M NaCl (HB10). **d**, Mander's coefficient of Rhodamine-labeled NOX overlapping each other labeled enzyme. This coefficient denotes the fraction of NOX that co-localizes with each of the other enzymes. In panels b and d, data represent the mean value and standard deviation (error bars) of , at least, 10 microbeads. For CLSM, enzymes were labeled with different fluorophores as follows; ADH1 (RhB, λ_{ex}: 561 nm, orange color), ADH2 (Atto 488, λ_{ex}: 488 nm, green color), LAC (Atto 390, λ_{ex}: 405 nm, blue color), CAT and NOX (A647, λ_{ex}: 633 nm, red color).

1 M NaCl was needed to locate NOX at the outer surface of the support, colonizing the outer 2% radius of the beads (2.5 µm on average) (**Figures 3b** and **S7**). **Figures 3c and S8** show the CLSM images that demonstrate the colocalization of the 5 enzymes at the outer region of the same bead. When 1 M NaCl is added to the immobilization buffer, the

Manders´s coefficients of NOX regarding the other enzymes (**Figure 3d, Table S1**) determined from the CLSM images confirm that NOX colocalizes with the rest of the enzymes to a higher extent than when NaCl was not added. As the support is positively charged, it can repel NOX, slowing its immobilization. Hence, we hypothesize that the chlorides will act as counter ions to the positive amine groups of AG-Co^{2+}/A/G, minimizing the repulsion and consequently immobilizing NOX faster on the outermost surface. The outer localization of NOX brings it closer to CAT, enhancing their cooperative action, but also increasing the NAD^+ recycling efficiency as the oxygen transport from the bulk to NOX is facilitated. The HB bearing the 5 enzymes colocalized at the outer surface of the beads will be now referred to as HB10 with a distribution 5 (D5) (**Entry 5, Table 1**). Furthermore, we corroborated that this new spatial location of NOX negligibly affects the immobilization pattern of the other enzyme members of the cascade (**Figure S8**).

Next, we evaluated the effect of the intraparticle NOX spatial distribution on biocatalyst productivity (**Figure 4a**) and operational stability (**Figure 4b**). First, we observe that the localization of NOX at the outer surface of the beads increases 5-HP titer upon 24 h reaction and maintains the chromatographic product yield (CY ≈ 70%) constant for 3 consecutive batch cycles unlike the HB9 (**Entry 4, Table 1**) where NOX is localized in the deeper surface of the porous support (**Figure 4b**). Unfortunately, the HB10 suffered operational inactivation in the 4^{th} operational cycle, observing a CY decay of 20%. To further increase the operational stability of HB10, we incubated the immobilized enzymes for longer times (16 h at 4 ºC) before the blocking step to fabricate HB11 (**Entry 6, Table 1**). Longer immobilization times pursue promoting the formation of more attachments between the residues at the enzyme surface and the aldehydes of AG-Co^{2+}/A/G, to ultimately improve the enzyme stability as reported elsewhere.[20] Nevertheless, the

increase in the immobilization time neither enhances the efficiency nor the operational stability of the HB11. Finally, to further optimize the performance of the HB10 biocatalyst, we increased the load of NOX and CAT by 4.7 and 7.25 times, respectively, resulting in a heterogeneous biocatalyst named HB12 with distribution D5 (**Entry 7, Table 1**). The specific activity of the immobilized NOX in HB12 decreased 1.8 times due to the higher protein density within the porous beads. Previous studies support the fact that NOX is less catalytically efficient at high protein loads, suggesting that protein crowding negatively affects the performance of this enzyme.[14] Despite this activity reduction, HB12 converted 100% 1,5-PD to yield 80% 5-HP (16 mM) after 24 h. Surprisingly, we observed 20% production (4 mM) of the 5-Oxopentanoic acid (5-OPA), indicating the overoxidation of the target 5-HP. This product overoxidation hints at a very efficient NAD^+-recycling system that boosts the oxidative activity of the two co-immobilized dehydrogenases (ADH1 and ADH2). This overoxidation is mainly attributed to the HLADH, which can catalyze the intermediate oxidation of 6-hydroxycaproic acid into 6-oxohexanoic acid during the synthesis of 6-aminocaproic acid (6ACA) from caprolactone. Regarding the operational stability, the excess of immobilized CAT drove to a less operationally stable biocatalyst as the product yield dramatically decayed to 10% upon re-using this biocatalyst in 5 consecutive batch cycles. In summary, the overall efficiency and operational stability of the 5-enzyme heterogeneous biocatalyst are optimized by localizing NOX at the outer surface of the beads and increasing the NOX and CAT loading in the biocatalyst, yet longer immobilization times negligibly improve the biocatalyst performance. To note, higher enzyme loads resulted in an HB less operationally stable. To understand whether the operational inactivation of HB12 relies on the enzyme lixiviation due to an excessive load, we performed an SDS-PAGE analysis of HB10-12. This electrophoretic analysis reveals that enzyme lixiviation similarly

occurred in all of them (**Figure S9**), thus operational inactivation may be triggered by the enzyme subunit leaching (quaternary structure disassembly) under reaction conditions, among other causes.

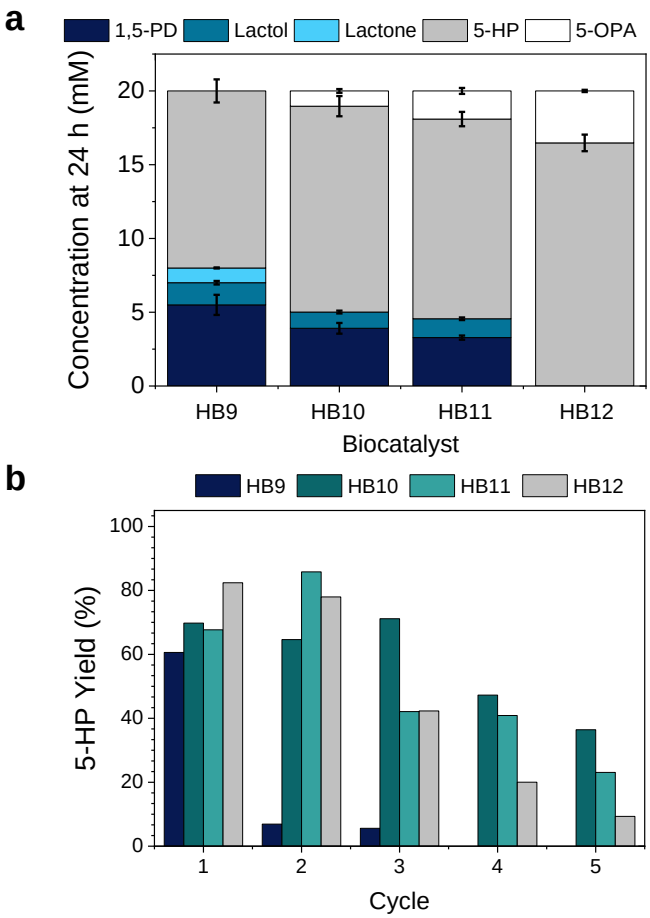

Figure 4. Effect of the NOX spatial distribution, immobilization time, and enzyme loading on the performance of different HBs for 5-HP biosynthesis in batch. **a,** 5-HP titer after 24 h reaction using HB9 (NOX in), HB10 (NOX out), HB11 (NOX out, 16 h immobilization), HB12 (higher loadings of NOX(out)/CAT). **b,** 5-HP yield after consecutive 24 h batch cycles using HB9-HB12. Reaction mixture: 20 mM 1,5-PD, 1 mM NAD^+, 0.15 mM FAD^+, 200 mM sodium phosphate buffer pH 8 at 30 ºC. Data in panel **a** corresponds to the mean value and standard deviation (error bars) of two independent experiments.

Improvement of the multi-functional heterogeneous biocatalysts by cationic polymer coating.

As most immobilized enzymes on HB12 are lixiviated during their operational use, we decided to stabilize their quaternary structure by polymer coating using polyallylamine (PAH). The enzyme coating with this cationic polymer enhances the performance of dehydrogenases and oxidases as previously reported by our group.[33] To that aim, after sequentially co-immobilizing the 5 enzymes with the optimal spatial distribution and enzyme loading, we coated them with PAH, fabricating a new version of HB12 named HB13 (**Entry 8, Table 1**). The primary amines of PAH react with the remaining aldehyde groups of the support not involved in enzyme attachment, acting as an ionic macromolecular crosslinker of enzyme subunits and as a blocking agent to make the support inert after the immobilization processes. This polymer coating increased the recovered activity of ADH1, ADH2, and NOX, suggesting that the aminated polymer has a stabilizing effect on the quaternary structure of the immobilized enzymes. SDS-PAGE analysis (**Figure S9, lanes 9 and 10**) confirms the stabilizing effect since enzyme subunits coated with PAG are lixiviated to a lower extent after consecutive batch cycles.

Next, we tested HB13 for the stepwise oxidation/hydrolysis of 1,5-PD into 5-HP in one pot. As a result, HB13 achieves a CY of 100% using 10 mM substrate in only 3 hours in comparison with the 80% conversion achieved with the same biocatalyst but blocked with glycine (HB12) (**Figures 5a** and **5b**). When the substrate load was scaled up to 20 mM, HB13 reached 90% CY in 6 hours (**Figure S10a**). Then, we studied the operational stability of HB13 by submitting it to consecutive recycling in 24 h batch cycles. **Figure 5c** shows how the PAH-coated heterogeneous biocatalyst was operationally stable for 4 consecutive cycles, while the substrate conversion decayed below 50% when using the non-coated HB12. This tendency is reflected also in the 5-HP yield along the cycles

(**Figure S10b**). Interestingly, we observed that HB13 maintains the 5-OPA yield after 4 consecutive cycles, whereas HB-12 was unable to produce such an overoxidized product in any analyzed cycle, as expected from its lower oxidation capacity (**Figure S10c**).

After successfully assembling a productive and stable multi-functional heterogeneous biocatalyst (HB13), we scaled the batch reaction volume up to 30 mL with 3.3% (w:v) biocatalyst load and monitored the product titer, the oxygen concentration, and the pH along the reaction course (**Figure S11**). As a pH decay occurs concomitantly to the 5-HP production, we manually kept the pH constant to a value of 8 by NaOH titration during the operation. The performance of HB13 in this scaled cascade is notorious as we achieved 80% 5-HP yield after 96 h operation, which means a product titer of 16.4 mM (c.a 0.5 mmol), a maximum volumetric productivity of 0.053 $g \cdot L^{-1} \cdot h^{-1}$ and a specific mass productivity of 1.1 $mg \cdot g_{HB13}^{-1} \cdot h^{-1}$. Furthermore, we observed a 6% reduction of the oxygen saturation in the reaction bulk during the first hour of the reaction. This oxygen depletion is related to the high rate of the first oxidative step (1,5-PD to lactol) associated with a very efficient NAD^+ regeneration system that concomitantly consumes molecular oxygen by the action of NOX. Then, the oxygen level increases until it reaches its steady saturation concentration (22%). This experimental evidence supports a very efficient coupling between ADH1 and its cofactor regeneration system (NOX/CAT).

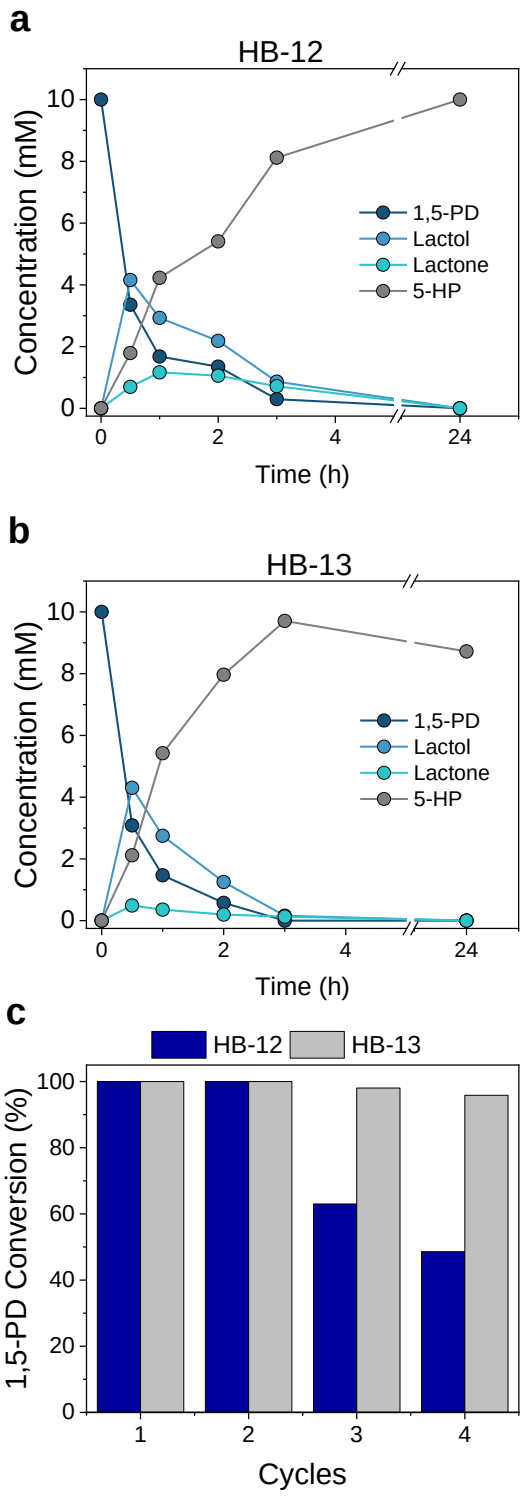

Figure 5. Effect of PAH coating on the performance of HBs for batch 5-HP biosynthesis. **a**, Reaction time courses using HB12 (without PAH coating) and **b**, HB13 (with PAH coating). **c**, Batch operational stability of HB12 and HB13 in consecutive cycles of 24 hours. All reaction mixes contained 10 mM 1,5-PD, 1 mM NAD^+, 0.15 mM FAD^+, and 200 mM sodium phosphate buffer pH 8 at 30 ºC. Data in all panels corresponds to the mean value and standard deviation (error bars) of two independent experiments.

Implementation of the optimal multi-functional heterogeneous biocatalyst in packed bed reactors for continuous synthesis of 5-HP.

In our efforts to intensify the process, we decided to integrate HB13 into a packed bed reactor (PBR). This PBR packed with 1 g of HB13 was first flushed with 10 mM 1,5-PD at 0.02 $mL \cdot min^{-1}$ showing no product formation. The UV-Vis spectra of samples collected from the PBR outlet demonstrated that the pool of redox cofactor was NADH (**Figure S12**), indicating the premature cascade halt due to inefficient NAD^+ recycling. Interestingly, the outlet samples were colorless indicating that FAD^+ was either absorbed to the surface of HB13 as reported for other heterogeneous biocatalysts coated with cationic polymers, or reduced to $FADH_2$ but not reoxidized due to the absence of oxygen.[34] This latter hypothesis is supported by the poor solubility of oxygen in the aqueous media (0.25 mM) and the lack of aeration within the PBR, explaining why the PBR fails to transform 1,5-PD into 5-HP due to the inefficient FAD^+ and NAD^+ *in-situ* regeneration. To overcome such a limitation, we flushed the PBR with an air-saturated solution but unfortunately neither did we detect the product.

Inspired by previous works from Nidetzky's[35] and Turner's[36] groups who managed to release soluble oxygen in a flow reactor flushing hydrogen peroxide in the presence of catalase, we decided to follow a similar approach to enhance NAD^+ recycling driven by NOX (**Figure 6a**). As HB13 integrates CAT, we run the PBR with this multi-functional heterogeneous biocatalyst using 20 mM 1,5-PD and varying H_2O_2 concentration at 0.01 $mL \cdot min^{-1}$ (**Figure 6b**). At 45 mM of H_2O_2, we achieved a maximum substrate conversion and product yield (CY) of 80% and 60%, respectively, determined by GC. However, at 90 mM H_2O_2, we observed a dramatic decay in the CY likely due to the harmful effect of

the hydrogen peroxide on enzyme stability. [37, 38] As expected, we also observed a linear correlation between the pH drop and the product titer at the reactor outlet, due to the

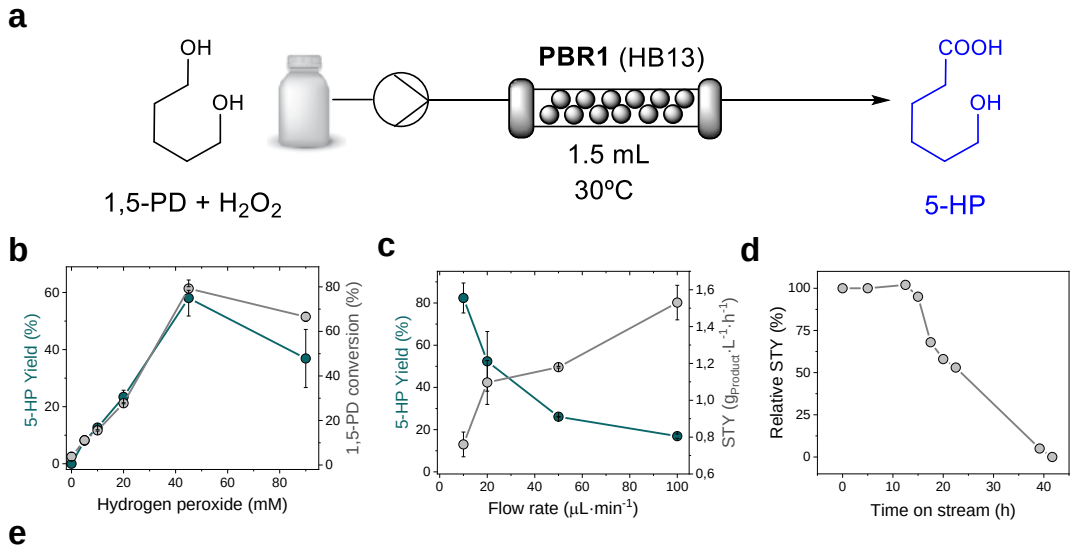

e

Flow rate (µl/min)	5-HP Yield (%)	R_T (min)	Space-Time Yield ($g_{Prodcut} \cdot L^{-1} \cdot h^{-1}$)	TOF ADH1 (h^{-1})	TOF ADH2 (h^{-1})	TOF LAC (h^{-1})	TTN_{NAD}	TTN_{FAD}
10	80,5 ± 7,1	150	0.76 ± 0.07	3019,3 ± 86,4	437,7 ± 25,7	6909,2 ± 406,5	34,1 ± 0,5	227,3 ± 3,3

Figure 6. Synthesis of 5-HP in flow catalyzed by a PBR packed with HB13. **a**, Scheme of the packed bed reactor. **b**, Product yield and substrate conversion at supplying a range of H_2O_2 concentrations. **c**, 5-HP, and STY at different flow rates. **d**, The evolution of STY along the operational time. Relative STY is defined as the percentage of STY regarding the initial STY at different times on the stream. **e**, Table of operational parameters under the optimal conditions. Turnover frequency (TOF) is defined as the mol of substrate converted per mol of enzyme per hour, being 1,5-PD the substrate for ADH1, lactol for ADH2, and lactone for LAC. Total turnover numbers (TTN) of cofactors (NAD^+ and FAD^+) are defined as the molar concentration of 5-HP x 2 divided by the molar concentration of each corresponding cofactor at the maximum STY. Data in panels **b**, **c**, and **e** represent the mean value and the standard deviation (error bars) of two independent experiments. Data in panel **c** corresponds to one operation run.

accumulation of higher concentrations of the target ω-hydroxy acid (**Figure S13**). To yield 20 mM product, the cascade demands 40 mM O_2 within the PBR. To reach that

oxygen concentration the flow reactor must be pressurized up to 30 bars according to the Henry law.[39,40] By feeding 45 mM H_2O_2 and 20 mM 1,5-PD, we theoretically supply the PBR with 42.5 mM of oxygen (22.5 mM directly from the fed H_2O_2, and 20 mM produced during the NAD^+ recycling) through the catalase-driven disproportionation of H_2O_2. In contrast, the same PBR fed with O_2 dissolved in reaction (aqueous) media under ambient pressure and 25 ºC is approximately 0.25 mM. Thus, the use of H_2O_2 as an oxygen supplier improves the safety of the process.

Once the optimal H_2O_2 concentration was found, we next challenged the PBR to a flow rate ramp to find its productivity limits. **Figure 6c** shows that the maximum product CY is achieved at the lowest flow rate, giving as a result the lowest STY. In contrast, the highest STY productivity occurred at a flow rate of 0.1 $mL \cdot min^{-1}$ at the expense of product titer with a CY as low as 18%. Thus, we selected 0.01 $mL \cdot min^{-1}$ and 45 mM H_2O_2 as the optimal conditions to operate the PBR. Under these conditions, we achieved 8.3 mM 5-HP in 150 min (residence time) with a STY = 0.76 ± 0.07 $g \cdot L^{-1} \cdot h^{-1}$ and a specific mass productivity of 0.76 $mg \cdot g_{HB13}^{-1} \cdot h^{-1}$ (**Figure 6c**). This latter parameter is slightly lower than that achieved with the 30 mL batch reactor under the same reaction conditions, suggesting that oxygen supply is still more efficient in a stirred tank than in an H_2O_2-fed PBR. Moreover, the ^{1}H-NMR of the sample collected directly from the outlet of the PBR shows a purer product than the sample separated from the batch process catalyzed by the free enzyme system (**Figure S14**). Under the optimal reaction conditions described above, the PBR was continuously operated for 44 h (**Figure 6d**). The STY was maintained during the first 12 h of operation and afterward steadily decreased to zero after 44 h of operation, detecting no product in the reactor outlet. *Post-used* and *ex-situ* activity assays revealed that the ADH activity of 44 h operated HB13 was 2 times lower than its

fresh counterpart. In contrast, NOX retained 90% of its initial activity in the exhausted biocatalysts. Therefore, the STY decay during the continuous operation is linked to the inactivation of the co-immobilized ADH1 and ADH2. This inactivation may be explained by an inefficient disproportionation of H_2O_2 due to the exhaustion of the catalase, accumulating H_2O_2 in the PBR. This accumulation can drive enzyme inactivation [37, 38] and carrier modification (i.e. cobalt chelates[41] or amine oxidation[42]) that ultimately limit the long-term operational stability of the multifunctional heterogeneous biocatalyst. This inactivation effect has been also observed in batch reactors using co-immobilized oxidases and catalases after several controlled additions of exogenous H_2O_2.[35]

Additionally, we calculated the turnover frequency (TOF) of each reaction step by analyzing the profiles of products and intermediates at the PBR outlet. **Figure 6e** shows that the rate-limiting step is the intermediate oxidation of the lactol to the lactone as the TOF of ADH2 is 7- and 16-fold lower than those of ADH1 and LAC, respectively. Remarkably, the generation of oxygen *in situ* is the most catalytically efficient step assuring the efficient recycling of the redox cofactor. Finally, the total turnover numbers (TTN) of cofactors were also determined, demonstrating that each molecule of NAD^+ and FAD^+ can be utilized up to 34 and 237 times, respectively, by ADHs and NOX.

Finally, we assessed the green and sustainability metrics of our heterogeneous biocatalysts (working in batch and in flow conditions) to be compared with their soluble counterparts (**Figure 7**). To that aim, we calculated the reaction mass efficiency (RME) and mass productivity (MP) defined as the mass of the product divided by either the mass of reactants or the total mass including catalysts and solvents, respectively. Secondly, we calculated the atom economy (AE) and the spatial time yield (STY) for the three compared systems. To this regard, we considered an ideal STY equal to 1 $g \cdot L^{-1} \cdot h^{-1}$, which is de minimum STY for high-priced products (**Figure 7a**).[43] The flow reactor improves

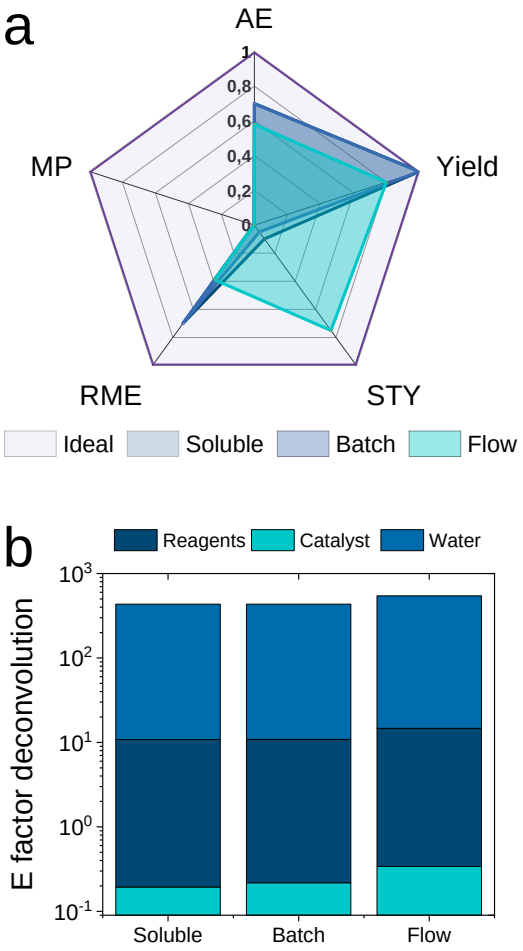

Figure 7. Green metric parameters of soluble and heterogeneous biocatalyst in the biosynthesis of 5-HP from 1,5-PD. **a**, AE = atom economy; MP = mass productivity; RME = Reaction mass efficiency; STY = space time yield (ideal STY corresponds to 1 $g \cdot L^{-1} \cdot h^{-1}$ which is de minimum STY for high-priced products). **b**, E factor deconvolution. Detailed reactor operation details are in **Table S2**.

the STY up to 7-fold compared to the batch systems but presents lower RME and AE due to the addition of H_2O_2. In all three systems, MP is the weakest parameter due to the large water excess required to achieve this biotransformation. Finally, we assessed the total E factor for the three reactor configurations (**Figure 7b**). All systems attained very similar E factors, indicating similar sustainability. It is worth mentioning that in the three cases, 97% of the E factor corresponds to water. Particularly, the contribution of the biocatalyst

is 150% higher in the flow reactor than in batch configurations either using free or immobilized enzymes.

Implementation of two telescoped PBRs for the biotransformation of 1,5-PD into 5-Aminopentanoic (5-AP) acid.

To further exploit the potential of this multi-functional heterogeneous biocatalyst, we studied its application in the biosynthesis of 5-Aminopentanoic (5-AP) acid. This ω-amino acid has gained attention for its potential use in nylon synthesis.[44, 45] To achieve this, we combined HB13 with a previously reported multi-functional heterogeneous biocatalyst (HB14)[45] for the conversion of 5-Hydroxypentanoic (5-HP) acid into 5-AP (**Figure 8a**). We assembled HB14 by co-immobilizing ADH2, NOX, and a transaminase from *Halomonas elongata* (HewT) on methacrylate beads. This support was functionalized with epoxy and aldehyde groups for the irreversible immobilization of ADH2, NOX, and HewT and further coated with polyethyleneimine (PEI) to improve the biocatalyst stabilization (**Figure S15a**). In contrast to our previous work,[45] we selected here an H_2O_2-forming NADH oxidase (NOX) encouraged by its excellent behavior as part of HB13 in flow reactors fed with H_2O_2. Immobilization yields were higher than 75% for all co-immobilized enzymes, whereas the recovered activities ranged from 3.5-65% depending on the enzyme, with being NOX the one that recovered the lowest activity (**Figure S15b**).

Once HB14 was fabricated, we packed HB13 and HB14 in two different PBRs and telescoped them for the continuous biotransformation of 1,5-PD into 5-AP (**Figure 8a**). Then, the continuous flow reaction was carried out in circulation mode at 0.02 $mL \cdot min^{-1}$, allowing the unreacted substrates to contact both PBRs for longer times. Remarkably, no additional air supply was needed for the PBR2 as the segmented air-liquid flow was naturally generated from the PBR1 by the action of CAT (**Figure 8a**, inlet). Isopropyl

amine (IPA) was added to the reaction mixture as an amine donor for the last transamination reaction. Under these conditions, 95% of 1,5-PD was consumed and 3.5

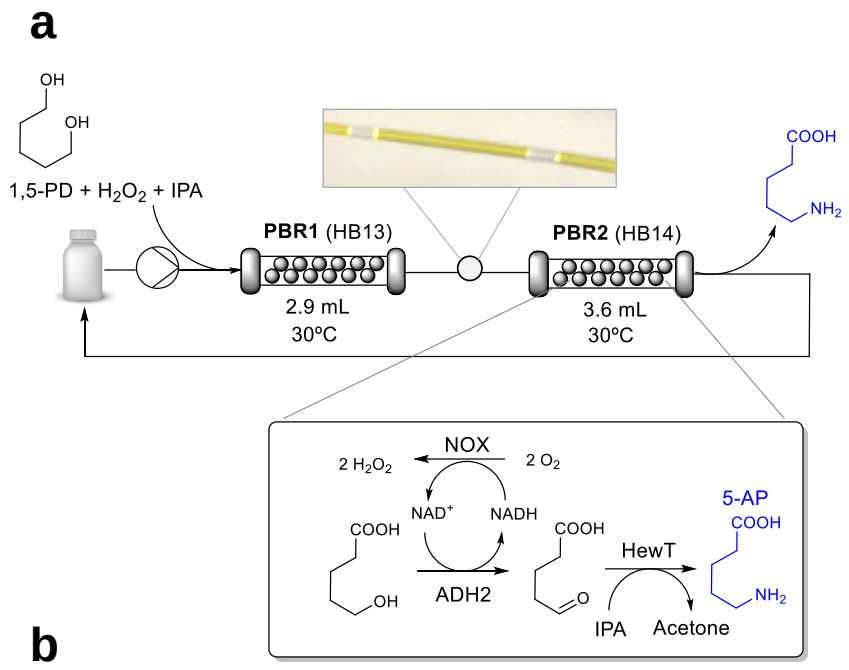

Circulation time	1,5-PD conversion	5-AP production	Coupling efficiency
(h)	(%)	(mM)	(mM 5-AP · mM 1,5-PD^{-1})
21	90.1	3.4	0.19
48	95.1	3.9	0.21
72	95.4	3.8	0.20

Figure 8. Continuous flow synthesis of 5-AP by telescoped packed-bed reactors. **a**, Scheme of the telescoped flow reaction set-up. The enzymatic cascade carried out in PBR1 is depicted in Figure 1a. PBR1 containing HB13 (1.7 g) was connected to PBR2 which was packed with HB14 (2.7 g). The flow biotransformation was performed in circulation mode (flow rate: 0.02 mL·min^{-1}) for 72 h. A segmented air-liquid flow occurred naturally between PBR1 and PBR2 due to the oxygen produced by PBR1. **b**, Time course of the telescoped reaction in flow. The reaction mix contained 20 mM 1,5-PD, 2 mM NAD^+, 1 mM FAD^+, 45 mM H_2O_2, 10 mM IPA, and 0.1 mM PLP in 100 mM sodium phosphate buffer pH 8. Data in panel **b** corresponds to one operation run.

mM of 5-AP was produced in 21 h (**Figure 8b**), which means 3 reactor cycles for PBR1 and PBR2, with a total residence time of 7.25 and 9 h, respectively. Longer reaction times

(up to 72 h) failed to increase the 5-AP titer, mainly due to the inactivation of the immobilized ADHs, whose activity decayed more than 70% upon their continuous operation (**Table S3**). To enhance the efficiency of this 6-enzyme 2-reactor system for the complete conversion of 1,5-PD into 5-AP in flow, we anticipate ongoing efforts. These include replacing ADHs with more robust ones, refining the immobilization strategy, and increasing the excess of amine donors.

CONCLUSION

In this work, we have immobilized a 5-enzymes cascade into porous supports as an artificial chassis to transform 1,ω-diols into either ω-hydroxy acids in one pot through a concurrent manner. Through a holistic approach and a deep characterization of the fabricated heterogeneous biocatalysts, we achieve a multi-functional heterogeneous biocatalyst with excellent reusability and capacity to be integrated into flow reactors. To that aim, we first tuned the spatial organization of the 5 enzymes involved in the cascade. Our findings indicate that the optimal spatial configuration is having the 5 enzymes co-immobilized on the same support bead and co-localized at its outermost region. The resulting heterogeneous biocatalyst underwent further optimization to enhance the efficiency of the NAD^+ recycling system with H_2O_2 removal *in situ*. Additionally, a cationic polymer coating was applied to the co-immobilized enzyme system, stabilizing their protein quaternary structures. This optimization journey resulted in a multi-functional heterogeneous biocatalyst denoted as HB13, which demonstrates excellent performance and operational stability. Specifically, HB13 was productive in the biosynthesis of 5-Hydroxypentanoic (5-HP) acid from 1,5-pentanediol (1,5-PD) under both discontinuous and continuous operation in batch and flow reactors, respectively.

In the transition of HB13 to packed-bed reactors (PBR) for continuous flow processing, we encountered a challenge to the inefficient reactor aeration under atmospheric pressure.

To overcome this limitation, we introduced H_2O_2 into the reactor to generate *in situ* the oxygen required by the NAD^+ recycling system driven by the NADH oxidase-catalase pair. The optimal spatial configuration and the robustness of these immobilized enzymes enable the utilization of up to 45 mM H_2O_2 within the HB13 porous particles. The flow transformation of diols into 5-HP reaches similar yields as those reached with whole-cells and cell-free systems transforming cyclic alkanes[23] and amines[24] into 5-HP. Volumetric productivities were not compared because the studies were performed at different substrate concentrations. Nonetheless, we made the effort to determine the green metrics of the optimized heterogeneous biocatalyst operated in batch and flow reactors. The continuous process results in higher productivity but slightly lower values of atom economy and mass productivities due to the exogenous supply of H_2O_2. Finally, HB13 packed into a PBR was telescoped with another PBR containing three co-immobilized enzymes, leading to the successful conversion of 1,5-PD into 5-Aminopentanoic acid (5-AP). This achievement, involving a total of six different enzymes spatially organized in two PBRs, sets a record for the number of enzymes (6) and reaction steps (7) assembled in a cell-free biosynthetic cascade operating in flow. Despite the involvement of oxygen-dependent enzymes, our approach demonstrated reasonable productivity.

Our work highlights the potential of strategically arranging immobilized enzymes to create more productive and complex heterogeneous biocatalytic systems, paving the way for the continuous biosynthesis of industrially relevant products. While the current system, with seven reactions catalyzed by six enzymes in two telescoped packed-bed reactors, may not be considered a complete cell-free metabolic pathway, we anticipate that further advancements in rational enzyme co-immobilization will contribute to expanding the capabilities of continuous chemical bio-manufacturing, enriching the bio-manufacturing portfolio.

METHODS

Materials: The enzymes, alcohol dehydrogenase from *Bacillus stearothermophilus* (ADH1), reduced nicotinamide adenine dinucleotide (NADH) oxidase from *Thermus thermophilus* HB27 (NOX), the lactonase from *Sulfolobus islandicus* (LAC), and the ω-transaminase from *Halomonas elongata* (HewT) were produced as previously reported.[25, 46] 6% crosslinked agarose (AG) beads (particle size 50−150 μm; pore diameter 300 nm) were purchased from Agarose Bead Technologies (Madrid, Spain). ReliSorb EP400/SS was acquired from Resindion S.R.L (Binasco, Italy). Compounds such as ethylenediamine (EDA), imidazole, iminodiacetic acid, cobalt chloride, sodium periodate, sodium hydroxide, Rhodamine B isothiocyanate, Atto 390 NHS ester, Atto 488 NHS ester, sodium acetate, sodium chloride, sodium phosphate, sodium bicarbonate, glutaraldehyde (GA), Poly(allylamine Mw: 65000 g mol^{-1}) (PAH), Poly(ethylenimine) Mw: 60000 g mol^{-1}) (PEI), Ampliflu™ Red, Protein Gel Stain, 1,5-pentanediol (1,5-PD), tetrahydro-2H-pyran-2-ol (lactol), δ-valerolactone (lactone), 5-Hydroxypentanoic (5-HP) acid, alcohol dehydrogenase from horse liver (ADH2), and pyridoxal-5'-phosphate (PLP), *S*-methylbenzyl amine (S-MBA) were acquired from Sigma-Aldrich Chemical Co. (St. Louis, IL). Alexa Fluor™ 647 NHS ester was purchased from Fisher Scientific. All other reagents were of analytical grade.

Enzyme Activity Assays. Enzyme activities were spectrophotometrically measured in transparent 96-well microplates with a flat bottom (Nunc), employing a Microplate Reader Epoch2 (BioTek Instruments) provided with the software Gen5.

ADH1 and ADH2 activity. Two hundred microliters of a reaction mixture containing 10 mM of 1,5-PD and 1 mM of NAD^+ in sodium phosphate buffer at pH 8 were incubated with 5 μL of enzymatic solution or 10 μL of immobilized enzyme suspension (properly diluted) at 30 °C. The increase in the absorbance at 340 nm due to the reduction of NAD^+ was recorded. One unit of activity was defined as the amount of enzyme that was required to reduce 1 μmol of NAD^+ to NADH per minute at the assayed conditions.

NOX activity. Two hundred microliters of a reaction mixture containing 0.2 mM of NADH and 150 μM of flavin adenine dinucleotide (FAD^+) in 50 mM sodium phosphate buffer pH 8 at 30 °C were incubated with 5 μL of enzymatic solution or 10 μL of immobilized enzyme suspension (properly diluted) at 30 °C. The oxidation of NADH was monitored as a decrease in the absorbance at 340 nm. One unit of activity was defined as the amount of enzyme that was required to oxidize 1 μmol of NADH to NAD^+ per minute at the assayed conditions.

CAT activity. Two hundred microliters of a reaction mixture containing 35 mM of hydrogen peroxide in 100 mM sodium phosphate pH 8 at 30 °C were incubated with 5 μL of the enzymatic solution or 10 μL of immobilized enzyme suspension (adequately diluted). The catalase activity was measured by recording the decrease in the absorbance at 240 nm. One unit of CAT activity was defined as the amount of enzyme required for the disproportionation of 1 μmol of hydrogen peroxide per minute at the assessed conditions.

LAC activity. Lactonase activity was indirectly monitored by the decrease in the pH triggered by the formation of 5-HP from its corresponding lactone hydrolysis. Briefly, 200 μL of a reaction mixture containing 1 mM δ-valerolactone, 0.1% acetonitrile, and 0.25 mM p-nitrophenol in 2.5 mM sodium phosphate buffer at pH 7.0 was incubated with 5 μL of enzymatic solution or 10 μL of immobilized enzyme suspension (properly

diluted) at 30 °C. The decrease in the absorbance of p-nitrophenol (pH indicator) at 410 nm was recorded. One unit of activity was defined as the amount of enzyme that was required to produce 1 μmol of 5-HP (titrated by pH change) per minute at the assayed conditions.

HewT activity. 5 μL of enzyme solution (0.5 mg·mL^{-1}) or 10 μL of immobilized enzyme suspension (1:20 w/v) were incubated with 200 μL containing 2.5 mM *S*-MBA, 2.5 mM pyruvate, and 0.1 mM PLP in 50 mM potassium phosphate buffer pH 8.0 at 30 ºC. Transaminase activity was monitored by recording the increase in absorbance at 245 nm for 5 min.

Synthesis of tri-heterofunctional Support (AG-Co^{2+}/A/G): We prepared AG functionalized with GA, EDA, and IDA/cobalt groups (AG-Co^{2+}/A/G) as described elsewhere.[25] Briefly, we prepared epoxy-activated agarose (AG-E), and then, we activated it with iminodiacetic acid (AG-E/IDA) by preparing a suspension of 10 g of AG-E in 100 mL of 0.5 mM iminodiacetic acid at pH 11 under gentle agitation at 200 rpm for 1 h at room temperature (RT). After filtering and rinsing with 10 volumes of water, AG-E/IDA was incubated with 10 volumes of 1 M ethylenediamine at pH 11 under gentle agitation at 200 rpm at room temperature overnight (AG-E/IDA/A). Afterward, the support was filtered and washed with 10 volumes of water, and then, incubated overnight with a 15% glutaraldehyde solution in a 200 mM sodium phosphate buffer pH 7 (AG-IDA/A/G) under gentle agitation at 200 rpm at room temperature. Subsequently, after filtering and washing, the support was incubated with 10 volumes of 30 mg·mL^{-1} of $CoCl_2$ for 2 h at room temperature (AG-Co^{2+}/A/G) Finally, the support was filtered and washed with abundant water and stored at 4 °C protected from light.

Optimization of the spatial organization in a heterogeneous 5-enzyme system

HB1-HB9: The assembly of heterogeneous biocatalysts was conducted by mixing 1 g of AG-Co^{2+}/A/G with 10 mL of each enzyme solution at the concentration shown in Table 1, dissolved in 100 mM sodium phosphate buffer at pH 7. Depending on the spatial distribution, the immobilization sequence differed (*vide infra*). In all cases, the enzyme-support suspension was maintained under gentle agitation at 25 rpm at 4 °C for 2 h. Subsequently, a blocking step was done to 1 g of immobilizate by adding 10 mL of 1 M glycine at pH 8. The suspension was incubated for 16 h at 25 rpm and 4 °C in a rotatory shaker. Once the immobilization was blocked, it was washed five times with five volumes of 25 mM sodium phosphate buffer pH 8, filtered, and stored at 4 °C. Specifically, for biocatalyst HB1 to HB5, each enzyme was individually immobilized. For co-immobilized systems, the immobilization process was conducted stepwise in the following order: HB-6: 1º NOX/CAT and 2º ADH1; HB-7: 1º NOX/CAT and 2º ADH2; HB-8: 1º NOX/CAT, 2º ADH1 and 3º ADH2; HB-9: 1º NOX/CAT, 2º ADH1, 3º ADH2 and 4º LAC. Between enzyme immobilization steps, immobilized samples were washed 3 times with five volumes of 25 mM sodium phosphate buffer pH 8 and filtered.

After the immobilization process, we calculated the immobilization yield (Ψ) corresponding to the amount of immobilized enzyme(s) on the solid support as described in equation 1;

Eq. 1

$$\Psi\% = \frac{\text{offered activity} - \text{activity in the supernatant}}{\text{offered activity}} x100$$

where offered activity is the initial activity of the soluble enzyme which was incubated with the support and the activity in the supernatant is the enzyme activity found in the filtrate of the enzyme suspension upon immobilization.

Likewise, we calculated the recovered activity (%) of the immobilized enzyme(s) in two ways, by calculating the total recovered activity per gram of solid support, and the percentage of specific recovered activity resulting after the immobilization process according to equation 2.

Eq. 2

$$Ar\ (\%) = \frac{\text{specific activity of the biocatalyst}}{\text{specific activity of the soluble enzyme}} x100$$

HB10: The assembly of a heterogeneous biocatalyst was conducted under the same conditions described above but in the case of NOX. After immobilizing all enzymes following the order 1º NOX in the presence of NaCl (0-1 M), 2º CAT/ADH2, 3º ADH1, 4º LAC. Finally, a blocking step was done by the addition of glycine (1 M, pH 8) followed by soft agitation overnight at 25 rpm and 4 °C.

HB11-HB13: The assembly of HB11, HB12, and HB13 was conducted as HB-10 with slight variation in the protocol. In the case of HB11, after the immobilization of the 5 enzymes, the immobilizate was incubated at 4 ºC overnight in sodium phosphate buffer pH 8, then it was blocked with 1 M glycine at 4 ºC for 3 h. In the case of HB12, we followed the same protocol as HB10 but loading 4 and 7 times more NOX and CAT, respectively (see entry 7, Table 1). In HB13, after the 5-enzyme immobilization, the immobilizate was incubated at 4 ºC overnight with 10 $mg \cdot mL^{-1}$ poly allylamine (PAH) in 25 mM HEPES buffer at pH 8.

Preparation of HB14: 3 g of EP400/SS microbeads were incubated with 30 mL of 0.1 M H_2SO_4 for 30 min. After filtration and washing with H_2O, 30 mL of $NaIO_4$ were added and the suspension was incubated for 2 h. After filtration and washing with H_2O, 30 mL

containing 12 mg of ADH2 (protein concentration determined by Bradford assay) and 15 mg of NOX in 0.1 M sodium bicarbonate buffer at pH 10.0 were added. The suspension was incubated for 1 h on ice. Then, 30 mg of $NaBH_4$ were added and the suspension was incubated for 30 min on ice. After filtration and washing with H_2O, 30 mL of 0.3 M EDA in 0.1 M sodium bicarbonate buffer at pH 8.5 was added and the suspension was incubated for 2 h. After filtration and washing with H_2O, 30 mL containing 15 mg of HewT in 50 mM potassium phosphate buffer at pH 8 was added. The suspension was incubated for 5 h on ice. Finally, 30 mL of a solution of 10 $mg \cdot mL^{-1}$ PEI (Mw 60000 mol g^{-1}) was added to block the remaining epoxy groups and the suspension was incubated for 16 h on ice.

Colorimetric assays to independently monitor intermediate reaction steps in the cascade.

Oxidative lactonization: Oxidative lactonization was monitored as shown in **Figure S2a**. Briefly, 200 µL of a reaction mixture containing 10 mM 1,5-PD and 1 mM of NAD^+ in 100 mM sodium phosphate buffer at pH 8 was incubated with 10 µL of suspension of HBs (properly diluted) at 30 ºC. The increase in the absorbance at 340 nm due to the reduction of NAD^+ was recorded. One unit of activity is defined as the reduction of 1 µmol of NAD^+ to NADH per minute at the assayed conditions.

Cofactor regeneration: Cofactor regeneration was monitored as shown in **Figure S2b**. Briefly, 200 µL of a reaction mixture containing 0.2 mM of NADH and 0.15 mM of FAD^+ in 100 mM sodium phosphate buffer at pH 8 was incubated with 10 µL of suspension of HBs (properly diluted) at 30 ºC. The increase in the absorbance at 340 nm due to the reduction of NAD^+ was recorded. One unit of activity is defined as the oxidation of 1 µmol of NADH to NAD^+ per minute at the assayed conditions.

Hydrogen peroxide accumulation: Hydrogen peroxide accumulation was monitored as shown in **Figure S3**.[47] Briefly, 200 μL of a reaction mixture containing 0.5 μg·mL^{-1} HRP, 20 mM 1,5-PD, 1 mM NAD^+, 0.15 mM FAD^+, 50 μM Ampliflu™ Red in 100 mM sodium phosphate buffer at pH 8 was incubated with 10 μL of suspension of HBs (properly diluted) at 30 ºC. The increase in the absorbance at 560 nm due to the formation of resorufin was recorded. One unit of activity is defined as the oxidation of 1 μmol of Ampliflu™ Red per minute at the assayed conditions.

ω-Hydroxy acid production: ω-Hydroxy acid production was monitored as shown in **Figure S4**.[48] Briefly, 200 μL of a reaction mixture containing 20 mM 1,5-PD, 1 mM NAD^+, 0.15 mM FAD^+, and 0.1 mM Cresol Red in 2.5 mM sodium phosphate buffer at pH 8 was incubated with 10 μL of suspension of HBs (properly diluted) at 30 ºC. The decrease in the absorbance at 580 nm due to the decrease in the pH was recorded. Also, the absorbance at 340 nm was recorded at the same time to guarantee that there is no NADH accumulation since it decreases the pH. One unit of activity is defined as 1 μmol H^+ (carboxylic group) per minute at the assayed conditions.

Enzyme Labeling with Fluorescent Probes. Fluorescent labeling of ADH1, ADH2, LAC, and CAT was done using a methodology reported elsewhere.[49] Each enzyme solution in 100 mM of sodium bicarbonate buffer at pH 8.5 (ADH1: 0.2 mg·mL^{-1}, ADH2: 1 mg·mL^{-1}, LAC: 1 mg·mL^{-1}, CAT: 3.9 mg·mL^{-1} and NOX: 1.2 mg·mL^{-1}) was mixed with the respective fluorophore: Rhodamine B (ADH1), Atto 488 (ADH2), Atto 390 (LAC and CAT) and A647 (NOX) at 1:1 molar ratio (stocks of each fluorophore were prepared in DMSO). The labeling reaction was then incubated for 2 hours under gentle shaking at 25 °C. Later, buffer exchange and removal of unreacted fluorophore was done by filtering the enzyme solution through a tangential ultrafiltration unit (10 kDa) equilibrated in 25 mM sodium phosphate buffered solution at pH 7.

Confocal Laser Scanning Microscopy (CLSM) Imaging. The localization and distribution of fluorophore-labeled immobilized enzymes for the different distributions were recorded with a Spectral ZEISS LSM 880 (Carl Zeiss, Germany) confocal microscope. Imaging was performed using 20x (0.8 NA) and 40x (immersion: water, 1.2 NA) objectives and different excitation lasers, λ_{ex}: 405 nm for Atto 390, λ_{ex}: 488 nm for Atto 488, λ_{ex}: 561 nm for Rhodamine B, and λ_{ex}: 633 nm for A647. All samples of each biocatalyst with the fluorescently labeled immobilized enzyme were suspended in an 8-well chamber slide (Ibidi) in a 1:200 (w:v) buffered suspension in 25 mM phosphate buffer at pH 7. The resulting micrographs were analyzed with FIJI software[50] to determine the relative infiltration radius and the colocalization parameters.[51]

Batch reactions to transform 1,5-PD into 5-HP catalyzed by different HBs. 100 mg of HB19 or a mix of HB1-8were placed inside a capped plastic tube (5 mL) containing 300 µL of a reaction mixture consisting of 20 mM of 1,5-PD, 1 mM of NAD^+, and 0.15 mM of FAD^+ in 100 mM sodium phosphate buffer pH 8 allowing atmospheric oxygen supplementation by punching the tap with an open needle. Reactions were incubated at 30 °C at 250 rpm inside an orbital incubator. The reaction course was monitored by withdrawing samples at periodic intervals, which were analyzed by chromatographic methods. In some experiments, this reaction was scaled up. To do so, 1 g of HB13 was placed inside a glass vessel (100 mL) containing 30 mL of a reaction mixture consisting of 20 mM of 1,5-PD, 1 mM of NAD^+, and 0.15 mM of FAD^+ in 100 mM sodium phosphate buffer pH 8 allowing atmospheric oxygen supplementation by agitation with impeller blades. The reaction was incubated at 30 °C at 600 rpm. Oxygen and pH were monitored continuously using an oximeter OXROB10 (Pyroscience, Aachen DE) and a pH meter (Mettler Toledo, Columbus, USA), respectively. The reaction progress was

monitored by withdrawing samples at periodic intervals and analyzing them by chromatographic methods.

Operational stability of HBs. Briefly, 100 mg of HBs were placed inside a capped plastic tube (5 mL) containing 300 μL of a reaction mixture consisting of 10-20 mM of 1,5-PD, 1 mM of NAD^+, and 0.15 mM of FAD^+ in 100 mM sodium phosphate buffer pH 8 allowing atmospheric oxygen supplementation by punching the tap with an open needle. Reactions were incubated at 30 °C at 250 rpm inside an orbital incubator and samples were collected at 24 hours. After each cycle, the HBs were washed once with 10 volumes of 100 mM sodium phosphate buffer at pH 8, and then mixed again with a fresh reaction media to start the following cycle.

Flow reactions to transform 1,5-PD into 5-HP catalyzed by HB13. The continuous flow biotransformations were conducted by packing 1 g of HB13 in a plastic plug-flow column and pumping through it a reaction mixture containing 20 mM of 1,5-PD, 1 mM of NAD^+, and 0.15 mM of FAD^+ (and additionally 0-90 mM of hydrogen peroxide) in 100 mM sodium phosphate buffer pH 8 with a syringe pump at 10-100 $\mu L \cdot min^{-1}$. Temperature was maintained at 30 ºC with a heated bath. The operational performance was monitored by withdrawing samples at periodic intervals and analyzing them by chromatographic and spectroscopic methods (*vide infra*).

Flow reactions to transform 1,5-PD into 5-AP catalyzed by HB13 and HB14. Flow biotransformations were performed using an R2S/R4 Vapourtec reactor equipped with two PBRs that were composed of an Omnifit glass column (6.6 mm i.d. ×100 mm length) packed with the immobilized enzymes. PBR1 contained 1.7 g of HB13 and PBR2 contained 2.7 g of HB14. Firstly, the system was equilibrated by pumping 100 mM sodium phosphate buffer pH 8.0 for 30 min. Secondly, a reaction mixture containing 20 mM 1,5-PD, 2 mM NAD^+, 1 mM FAD^+, 45 mM hydrogen peroxide, 10 mM IPA, and 0.1

mM PLP in 100 mM sodium phosphate buffer pH 8 was passed through the PBRs using an R2S pump. The reaction mixture was pumped at a flow rate of 0.02 mL·min^{-1} at 30 °C until it reached the outlet of the PBR2. At this point, the output was fed back into the recipient containing the reaction mixture, and the reaction was run in circulation mode at 30 °C for 72 h (corresponding to 10.6 passes). Samples were collected after 21, 48, and 72 h and analyzed by GC and HPLC (*vide infra*).

High-performance liquid chromatography (HPLC) analysis. The detection of 5-amino valeric acid (5-AP) was performed by FMOC derivatization as previously described.[45] 50 µL of the biotransformation were added to 100 µL of 100 mM borate buffer at pH 9.0 and 200 µL of 15 mM FMOC in acetonitrile (ACN). After 5 minutes, 50 µL of the FMOC-derivatized sample was mixed with 200 µL of 0.2% HCl in H_2O and 200 µL of ACN and filtered with a 0.45 µm PTFE filter. The samples were analyzed by HPLC Dionex UltiMate 3000 (Thermo Fisher, Loughborough, UK), equipped with a C18 column (3.5 µm, 2.1×100 mm) (Waters, Elstree, UK). 2 µL of the sample were injected and analyzed using a gradient method 5:95 to 95:5 (H_2O/ACN containing 0.1 % trifluoracetic acid) over 4 minutes with a flow rate of 0.8 mL·min^{-1} at 45 °C. The FMOC-derivatized 5-AP (6.37 min) was detected using UV detectors at 265 nm. Molar conversions were calculated with a calibration curve of 5-AP.

Gas chromatography (GC) analysis. (Extraction) Before GC analysis, 50 µL of the reaction sample was mixed with 200 µL of ethyl acetate to perform a liquid−liquid extraction of the compounds of interest containing 2 mM eicosane as an external standard. After the extraction, 30−50 mg of anhydrous $MgSO_4$ was added to dry samples before GC analysis.[52] (Derivatization) All reaction samples were derivatized as described elsewhere.[22] Additionally, 50 µL of aqueous reaction sample was placed in a 1.5 mL Eppendorf tube. Later, 150 µL of ethyl acetate was added and vortexed for 20 s, then 20–

50 mg of anhydrous $MgSO_4$ were added to dry samples before GC analysis using eicosane 2 mM as external standard. Gas chromatography analyses were carried out in an Agilent 8890GC system chromatograph using a J&WHP-5GC column (30 m × 0.32 mm ×0.25 μm), helium as the support gas, and equipped with a flame ionization detector (FID). The injector asset at 280 °C and the FID at 300 °C. The injection volume of 1 μL with a split ratio of 10. Separation of extracted compounds in ethyl acetate was done by the following temperature program: the initial temperature at 60 °C, maintained 2 min, ramp to 160 °C at a rate of 10 °C·min^{-1}, ramp 2−240 °C at a rate of 20 °C·min^{-1} and finally maintained 4 min.

Nuclear magnetic resonance (NMR) analysis. When specified, reaction samples were analyzed by ^{1}H NMR spectra acquired on a Bruker 500 MHz Ultra Shield spectrometer, operating at 500 MHz for ^{1}H NMR spectroscopy. Chemical shifts (δ) were reported in parts-per-million (ppm) and referenced using the residual solvent peak (deuterium oxide; δ=4.79 ppm). Coupling constants (J) were reported in hertz (Hz). The multiplicity of the signals was reported as singlet(s), doublet(d), doublet of doublets of doublets of doublets (dddd), doublet of the quartet (dq), doublet of triplet (dt), triplet (t), and multiplet (m).

ACKNOWLEDGMENTS

ERC-Co (METACELL-818089), and RETOS (SOMECS-RTI2018-094398-B-I00) projects are acknowledged for funding. FLG thanks IKERBASQUE for sponsoring him. SVL acknowledges the funding from ARAID. JSA thanks the FPI fellowship program of the Spanish Research Agency (PRE2019-090835) This work was performed under the Maria de Maeztu Units of Excellence Program from the Spanish State Research Agency—grant no. MDM-2017-0720 (CIC biomaGUNE). FP and AIBM acknowledge

the support from the SNSF (grant: 200021_192274) and the University of Bern (SELF19-03 BIORPHANDRUG).

SUPPLEMENTARY INFORMATION

The Supplementary Information is available free of charge. Supplementary content includes schemes of colorimetric assays and spatial distribution, supporting CLSM images, SDS-PAGE, 30-mL scale batch reaction, ^{1}H-NMRs of products, and UV-Vis spectra. Raw data of colocalization studies and green metrics analysis.

CONFLICT OF INTEREST

There are no conflicts to declare.

REFERENCES

(1) Rasor, B. J.; Vögeli, B.; Landwehr, G. M.; Bogart, J. W.; Karim, A. S.; Jewett, M. C., Toward sustainable, cell-free biomanufacturing. *Curr. Opin. Biotechnol.* **2021,** *69*, 136-144.
(2) Huffman, M. A.; Fryszkowska, A.; Alvizo, O.; Borra-Garske, M.; Campos, K. R.; Canada, K. A.; Devine, P. N.; Duan, D.; Forstater, J. H.; Grosser, S. T.; Halsey, H. M.; Hughes, G. J.; Jo, J.; Joyce, L. A.; Kolev, J. N.; Liang, J.; Maloney, K. M.; Mann, B. F.; Marshall, N. M.; McLaughlin, M.; Moore, J. C.; Murphy, G. S.; Nawrat, C. C.; Nazor, J.; Novick, S.; Patel, N. R.; Rodriguez-Granillo, A.; Robaire, S. A.; Sherer, E. C.; Truppo, M. D.; Whittaker, A. M.; Verma, D.; Xiao, L.; Xu, Y.; Yang, H., Design of an in vitro biocatalytic cascade for the manufacture of islatravir. *Science* **2019,** *366* (6470), 1255-1259.
(3) Guterl, J. K.; Garbe, D.; Carsten, J.; Steffler, F.; Sommer, B.; Reisse, S.; Philipp, A.; Haack, M.; Ruhmann, B.; Koltermann, A.; Kettling, U.; Bruck, T.; Sieber, V., Cell-free metabolic engineering: production of chemicals by minimized reaction cascades. *ChemSusChem* **2012,** *5* (11), 2165-72.
(4) Wang, Z.; Sundara Sekar, B.; Li, Z., Recent advances in artificial enzyme cascades for the production of value-added chemicals. *Bioresour. Technol.* **2021,** *323*, 124551.
(5) Faber, K.; Fessner, W.-D.; Turner, N. J., Engineering Biocatalysts for Synthesis Including Cascade Processes. *Adv. Synth. Catal.* **2015,** *357* (8), 1565-1566.
(6) Guisan, J. M.; López-Gallego, F.; Bolivar, J. M.; Rocha-Martín, J.; Fernandez-Lorente, G., The Science of Enzyme Immobilization. In *Immobilization of Enzymes and Cells: Methods and Protocols*, Guisan, J. M.; Bolivar, J. M.; López-Gallego, F.; Rocha-Martín, J., Eds. Springer US: New York, NY, 2020; pp 1-26.
(7) Sheldon, R. A.; Brady, D., The limits to biocatalysis: pushing the envelope. *Chem. Commun.* **2018,** *54* (48), 6088-6104.
(8) Crotti, M.; Robescu, M. S.; Bolivar, J. M.; Ubiali, D.; Wilson, L.; Contente, M. L., What's new in flow biocatalysis? A snapshot of 2020–2022. *Front. Catal.* **2023,** *3*.

(9) Santi, M.; Sancineto, L.; Nascimento, V.; Braun Azeredo, J.; Orozco, E. V. M.; Andrade, L. H.; Gröger, H.; Santi, C., Flow Biocatalysis: A Challenging Alternative for the Synthesis of APIs and Natural Compounds. *Int. J. Mol. Sci.* **2021,** *22* (3), 990.
(10) De Santis, P.; Meyer, L.-E.; Kara, S., The rise of continuous flow biocatalysis – fundamentals, very recent developments and future perspectives. *React. Chem. Eng.* **2020,** *5* (12), 2155-2184.
(11) Romero-Fernández, M.; Paradisi, F., Protein immobilization technology for flow biocatalysis. *Curr. Opin. Chem. Biol.* **2020,** *55*, 1-8.
(12) Roura Padrosa, D.; Benítez-Mateos, A. I.; Paradisi, F., Flow Biocatalysis for Chiral Molecules Synthesis. In *Reference Module in Chemistry, Molecular Sciences and Chemical Engineering*, Elsevier: 2023.
(13) Contente, M. L.; Farris, S.; Tamborini, L.; Molinari, F.; Paradisi, F., Flow-based enzymatic synthesis of melatonin and other high value tryptamine derivatives: A five-minute intensified process. *Green Chem.* **2019,** *21* (12), 3263-3266.
(14) Benítez-Mateos, A. I.; Huber, C.; Nidetzky, B.; Bolivar, J. M.; López-Gallego, F., Design of the Enzyme–Carrier Interface to Overcome the O 2 and NADH Mass Transfer Limitations of an Immobilized Flavin Oxidase. *ACS Appl. Mater. Interfaces* **2020,** *12* (50), 56027-56038.
(15) Rocha-Martin, J.; Acosta, A.; Guisan, J. M.; López-Gallego, F., Immobilizing Systems Biocatalysis for the Selective Oxidation of Glycerol Coupled to In Situ Cofactor Recycling and Hydrogen Peroxide Elimination. *ChemCatChem* **2015,** *7* (13), 1939-1947.
(16) Benítez-Mateos, A. I.; Bertella, S.; Behaghel de Bueren, J.; Luterbacher, J. S.; Paradisi, F., Dual Valorization of Lignin as a Versatile and Renewable Matrix for Enzyme Immobilization and (Flow) Bioprocess Engineering. *ChemSusChem* **2021,** *14* (15), 3198-3207.
(17) Rodrigues, R. C.; Virgen-Ortíz, J. J.; dos Santos, J. C. S.; Berenguer-Murcia, Á.; Alcantara, A. R.; Barbosa, O.; Ortiz, C.; Fernandez-Lafuente, R., Immobilization of lipases on hydrophobic supports: immobilization mechanism, advantages, problems, and solutions. *Biotechnol. Adv.* **2019,** *37* (5), 746-770.
(18) Zaak, H.; Sassi, M.; Fernandez-Lafuente, R., A new heterofunctional amino-vinyl sulfone support to immobilize enzymes: Application to the stabilization of β-galactosidase from Aspergillus oryzae. *Process Biochem.* **2018,** *64*, 200-205.
(19) Albuquerque, T. L. d.; Rueda, N.; dos Santos, J. C. S.; Barbosa, O.; Ortiz, C.; Binay, B.; Özdemir, E.; Gonçalves, L. R. B.; Fernandez-Lafuente, R., Easy stabilization of interfacially activated lipases using heterofunctional divinyl sulfone activated-octyl agarose beads. Modulation of the immobilized enzymes by altering their nanoenvironment. *Process Biochem.* **2016,** *51* (7), 865-874.
(20) Rodrigues, R. C.; Berenguer-Murcia, Á.; Carballares, D.; Morellon-Sterling, R.; Fernandez-Lafuente, R., Stabilization of enzymes via immobilization: Multipoint covalent attachment and other stabilization strategies. *Biotechnol. Adv.* **2021,** *52*, 107821.
(21) Kienle, D. F.; Chaparro Sosa, A. F.; Kaar, J. L.; Schwartz, D. K., Polyelectrolyte Multilayers Enhance the Dry Storage and pH Stability of Physically Entrapped Enzymes. *ACS Appl. Mater. Interfaces* **2020,** *12* (20), 22640-22649.
(22) Velasco-Lozano, S.; Santiago-Arcos, J.; Grazia Rubanu, M.; López-Gallego, F., Cell-Free Biosynthesis of ω-Hydroxy Acids Boosted by a Synergistic Combination of Alcohol Dehydrogenases. *ChemSusChem* **2022,** *15* (9), e202200397.
(23) Salamanca, D.; Bühler, K.; Engesser, K.-H.; Schmid, A.; Karande, R., Whole-cell biocatalysis using the Acidovorax sp. CHX100 Δ6HX for the production of ω-hydroxycarboxylic acids from cycloalkanes. *N. Biotechnol.* **2021,** *60*, 200-206.
(24) Sarak, S.; Sung, S.; Jeon, H.; Patil, M. D.; Khobragade, T. P.; Pagar, A. D.; Dawson, P. E.; Yun, H., An Integrated Cofactor/Co-Product Recycling Cascade for the Biosynthesis of Nylon Monomers from Cycloalkylamines. *Angew. Chem. Int. Ed.* **2021,** *60* (7), 3481-3486.
(25) Santiago-Arcos, J.; Velasco-Lozano, S.; López-Gallego, F., Multienzyme Coimmobilization on Triheterofunctional Supports. *Biomacromolecules* **2023,** *24* (2), 929-942.
(26) Ceccarelli, C.; Liang, Z.-X.; Strickler, M.; Prehna, G.; Goldstein, B. M.; Klinman, J. P.; Bahnson, B. J., Crystal Structure and Amide H/D Exchange of Binary Complexes of Alcohol

Dehydrogenase from Bacillus stearothermophilus: Insight into Thermostability and Cofactor Binding. *Biochemistry* **2004,** *43* (18), 5266-5277.
(27) Adolph, H.-W.; Zwart, P.; Meijers, R.; Hubatsch, I.; Kiefer, M.; Lamzin, V.; Cedergren-Zeppezauer, E., Structural Basis for Substrate Specificity Differences of Horse Liver Alcohol Dehydrogenase Isozymes†. *Biochemistry* **2000,** *39* (42), 12885-12897.
(28) Rocha-Martín, J.; Vega, D.; Bolivar, J. M.; Godoy, C. A.; Hidalgo, A.; Berenguer, J.; Guisán, J. M.; López-Gallego, F., New biotechnological perspectives of a NADH oxidase variant from Thermus thermophilus HB27 as NAD+-recycling enzyme. *BMC Biotechnol.* **2011,** *11* (1), 101.
(29) Hiblot, J.; Gotthard, G.; Chabriere, E.; Elias, M., Structural and Enzymatic characterization of the lactonase SisLac from Sulfolobus islandicus. *PLOS ONE* **2012,** *7* (10), e47028.
(30) Velasco-Lozano, S.; Santiago-Arcos, J.; Mayoral, J. A.; López-Gallego, F., Co-immobilization and Colocalization of Multi-Enzyme Systems for the Cell-Free Biosynthesis of Aminoalcohols. *ChemCatChem* **2020,** *12* (11), 3030-3041.
(31) NOTE, K_M values of ADH1, ADH2 and LAC toward 1,5-PD, lactol and δ-valerolactone are 1.29 mM, 1.54 M and 19.06 mM, respectively.
(32) Bolivar, J. M.; Hidalgo, A.; Sanchez-Ruiloba, L.; Berenguer, J.; Guisan, J. M.; Lopez-Gallego, F., Modulation of the distribution of small proteins within porous matrixes by smart-control of the immobilization rate. *J. Biotechnol.* **2011,** *155* (4), 412-20.
(33) Diamanti, E.; Santiago-Arcos, J.; Grajales-Hernández, D.; Czarnievicz, N.; Comino, N.; Llarena, I.; Di Silvio, D.; Cortajarena, A. L.; López-Gallego, F., Intraparticle Kinetics Unveil Crowding and Enzyme Distribution Effects on the Performance of Cofactor-Dependent Heterogeneous Biocatalysts. *ACS Catal.* **2021,** *11* (24), 15051-15067.
(34) Gurruchaga-Pereda, J.; Martínez-Martínez, V.; Rezabal, E.; Lopez, X.; Garino, C.; Mancin, F.; Cortajarena, A. L.; Salassa, L., Flavin Bioorthogonal Photocatalysis Toward Platinum Substrates. *ACS Catal.* **2020,** *10* (1), 187-196.
(35) Schelch, S.; Bolivar, J. M.; Nidetzky, B., Monitoring and control of the release of soluble O2 from H2O2 inside porous enzyme carrier for O2 supply to an immobilized d-amino acid oxidase. *Biotechnol. Bioeng.* **2022,** *119* (9), 2374-2387.
(36) Chapman, M. R.; Cosgrove, S. C.; Turner, N. J.; Kapur, N.; Blacker, A. J., Highly Productive Oxidative Biocatalysis in Continuous Flow by Enhancing the Aqueous Equilibrium Solubility of Oxygen. *Angew. Chem. Int. Ed.* **2018,** *57* (33), 10535-10539.
(37) Stadtman, E. R.; Levine, R. L., Free radical-mediated oxidation of free amino acids and amino acid residues in proteins. *Amino Acids* **2003,** *25* (3-4), 207-18.
(38) Hernandez, K.; Berenguer-Murcia, A.; C. Rodrigues, R.; Fernandez-Lafuente, R., Hydrogen Peroxide in Biocatalysis. A Dangerous Liaison. *Curr. Org. Chem.* **2012,** *16* (22), 2652-2672.
(39) $[O_2] = P \times K$; $K_L(O_2) = 1.3 \times 10^{-3}$ (20 ºC)
(40) Bolivar, J. M.; Mannsberger, A.; Thomsen, M. S.; Tekautz, G.; Nidetzky, B., Process intensification for O2-dependent enzymatic transformations in continuous single-phase pressurized flow. *Biotechnol. Bioeng.* **2019,** *116* (3), 503-514.
(41) Wegner, S. V.; Schenk, F. C.; Spatz, J. P., Cobalt(III)-Mediated Permanent and Stable Immobilization of Histidine-Tagged Proteins on NTA-Functionalized Surfaces. *Chem. Eur. J.* **2016,** *22* (9), 3156-3162.
(42) Sato, K.; Takahashi, M.; Ito, M.; Abe, E.; Anzai, J.-i., H2O2-Induced Decomposition of Layer-by-Layer Films Consisting of Phenylboronic Acid-Bearing Poly(allylamine) and Poly(vinyl alcohol). *Langmuir* **2014,** *30* (31), 9247-9250.
(43) Meissner, M. P.; Woodley, J. M., Mass-based biocatalyst metrics to guide protein engineering and bioprocess development. *Nat. Catal.* **2022,** *5* (1), 2-4.
(44) Joo, J. C.; Oh, Y. H.; Yu, J. H.; Hyun, S. M.; Khang, T. U.; Kang, K. H.; Song, B. K.; Park, K.; Oh, M.-K.; Lee, S. Y.; Park, S. J., Production of 5-aminovaleric acid in recombinant Corynebacterium glutamicum strains from a Miscanthus hydrolysate solution prepared by a newly developed Miscanthus hydrolysis process. *Bioresour. Technol.* **2017,** *245*, 1692-1700.

(45) Romero-Fernandez, M.; Heckmann, C. M.; Paradisi, F., Biocatalytic Production of a Nylon 6 Precursor from Caprolactone in Continuous Flow. *ChemSusChem* **2022,** *15* (16), e202200811.
(46) Cerioli, L.; Planchestainer, M.; Cassidy, J.; Tessaro, D.; Paradisi, F., Characterization of a novel amine transaminase from Halomonas elongata. *J. Mol. Catal. B: Enzym.* **2015,** *120*, 141-150.
(47) Morlock, L. K.; Böttcher, D.; Bornscheuer, U. T., Simultaneous detection of NADPH consumption and H2O2 production using the Ampliflu™ Red assay for screening of P450 activities and uncoupling. *Appl. Microbiol. Biotechnol.* **2018,** *102* (2), 985-994.
(48) Camacho-Ruiz, M. A.; Müller-Santos, M.; Hernández-Mancillas, X. D.; Armenta-Perez, V. P.; Zamora-Gonzalez, E.; Rodríguez, J. A., A sensitive pH indicator-based spectrophotometric assay for PHB depolymerase activity on microtiter plates. *Analytical Methods* **2020,** *12* (32), 4048-4057.
(49) Holmes, K. L.; Lantz, L. M., Chapter 9 Protein labeling with fluorescent probes. In *Methods Cell. Biol.*, Academic Press: 2001; Vol. 63, pp 185-204.
(50) Schindelin, J.; Arganda-Carreras, I.; Frise, E.; Kaynig, V.; Longair, M.; Pietzsch, T.; Preibisch, S.; Rueden, C.; Saalfeld, S.; Schmid, B., Fiji: an open-source platform for biological-image analysis. *Nat. Methods* **2012,** *9* (7), 676-682.
(51) Diamanti, E.; Arana-Peña, S.; Ramos-Cabrer, P.; Comino, N.; Carballares, D.; Fernandez-Lafuente, R.; López-Gallego, F., Intraparticle Macromolecular Migration Alters the Structure and Function of Proteins Reversibly Immobilized on Porous Microbeads. *Adv. Mater. Interf.* **2022,** *9* (18).
(52) Huang, L.; Bittner, J. P.; Domínguez de María, P.; Jakobtorweihen, S.; Kara, S., Modeling Alcohol Dehydrogenase Catalysis in Deep Eutectic Solvent/Water Mixtures. *ChemBioChem* **2020,** *21* (6), 811-817.

GRAPHICAL ABSTRACT

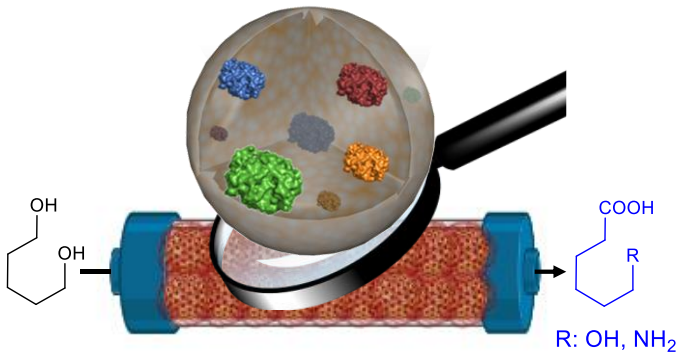

Controlling spatial organization of co-immobilized 5/6 enzymes on porous microbeads allows the intensification of the transformation of 1,omega-diols into 1,omega-hydroxy/amino acids.